

THESIS FOR THE DEGREE OF DOCTOR OF PHILOSOPHY

**Mechanism of the passive NO_x adsorption
process on zeolite-supported Pd in
controlling cold-start emissions**

Rojin Feizie Ilmasani

Department of Chemistry and Chemical Engineering

CHALMERS UNIVERSITY OF TECHNOLOGY

Gothenburg, Sweden 2022

Mechanism of the passive NO_x adsorption process on zeolite-supported Pd in controlling cold-start emissions

Rojin Feizie Ilmasani

ISBN: 978-91-7905-634-6

© Rojin Feizie Ilmasani, 2022.

Doktorsavhandlingar vid Chalmers tekniska högskola

Ny series nr 5100

ISSN 0346-718X

Department of Chemistry and Chemical Engineering

Chalmers University of Technology

SE-412 96 Gothenburg

Sweden

Telephone + 46 (0)31-772 1000

Cover:

Mechanism of the passive NO_x adsorption process on Pd/zeolite in emissions control

Printed by Chalmers Digitaltryck

Gothenburg, Sweden 2022

Mechanism of the passive NO_x adsorption process on zeolite-supported Pd in controlling cold-start emissions

Rojin Feizie Ilmasani

Department of Chemistry and Chemical Engineering
Chalmers University of Technology, Gothenburg, Sweden 2022

Abstract

Passive NO_x adsorbents (PNA) can be used for preventing that NO_x emissions are released during cold start. This method involves trapping NO_x on an adsorbent at low temperatures and releasing them later, when the exhaust temperature exceeds 200°C. One of the well-known adsorbents used in PNA is Pd on zeolites, due to its high storage capacity of NO_x.

In this work, La was found to promote Pd/BEA by increasing the desorption temperature of NO_x above 200°C compared to the reference material. DRIFTS analysis showed the formation of more stable NO_x species during adsorption with La-modified Pd/BEA, thereby improving the thermal stability. In addition, La-promoted Pd/BEA, unlike non-promoted Pd/BEA, showed increased performance stability after multiple cycles of NO-TPD experiments with elevated levels of CO in the inlet gas. Different characterization techniques, indicated the formation of less agglomerated Pd clusters on the zeolite framework in the La modified sample after multiple cycles, which led to a more stable performance. A study of the deactivation mechanism of CO on Pd/SSZ-13 indicated that the agglomeration mechanism of Pd consists of two sintering modes: Ostwald ripening in the first cycles of NO-TPD, followed by particle migration in the later cycles. On the other hand, low concentrations of CO shifted the NO_x release peaks towards more favourable temperature ranges in Pd/SSZ-13. XPS analysis was used to investigate the positive effects of low CO levels and showed that the Pd species were reduced by CO adsorption which, in turn, increased the NO_x binding strength.

Moreover, the presence of phosphorous on Pd/SSZ-13 caused a reduction in the efficiency of the adsorbent: this deactivation was more severe when the phosphorous content was increased. The formation of three main phosphorous species were observed: phosphorus pentoxide (P₂O₅), which causes physical deactivation of Pd/SSZ-13, and metaphosphate (PO₃⁻) and phosphate (PO₄³⁻), both of which cause chemical deactivation. Different characterization techniques revealed that it is the interaction of P with Pd and the zeolite framework that caused this chemical deactivation. Moreover, it was found that the BET surface area and pore volume of Pd/SSZ-13 were reduced due to physical blockage caused by phosphorous pentoxide species.

Keywords: *Passive NO_x adsorber, Pd/zeolite, La promotion, thermal stability, multiple NO-TPD, CO effect and degradation, phosphorous poisoning*

List of publications

I. **Influencing the NO_x stability by metal oxide addition to Pd/BEA for passive NO_x adsorbers**

Rojin Feizie Ilmasani, Jungwon Woo, Derek Creaser, Louise Olsson
Industrial & Engineering Chemistry Research 2020, 59, 9830 – 9840.
<https://doi.org/10.1021/acs.iecr.9b06976>

II. **Investigation of CO deactivation of passive NO_x adsorption on La promoted Pd/BEA**

Rojin Feizie Ilmasani, Phuoc Hoang Ho, Aiyong Wang, Dawei Yao, Derek Creaser, Louise Olsson
Emission Control Science and Technology, Published 2021. <https://doi.org/10.1007/s40825-021-00205-2>

III. **Kinetic modeling of CO assisted passive NO_x adsorption on Pd/SSZ-13**

Dawei Yao, Rojin Feizie Ilmasani, Johannes Wurzenberger, Thomas Glatz, Joonsoo Han, Aiyong Wang, Derek Creaser, Louise Olsson
Chemical Engineering Journal, Published 2022. <https://doi.org/10.1016/j.cej.2021.132459>

IV. **Kinetic modeling of CO induced degradation of Pd/zeolite during NO_x storage and release**

Dawei Yao, Rojin Feizie Ilmasani, Johannes Wurzenberger, Thomas Glatz, Joonsoo Han, Hoang Phuoc Ho, Derek Creaser, Louise Olsson
Submitted.

V. **Deactivation study of phosphorous-poisoned Pd/SSZ-13 in the passive adsorption of NO_x**

Rojin Feizie Ilmasani, Dawei Yao, Phuoc Hoang Ho, Diana Bernin, Derek Creaser, Louise Olsson
Submitted.

Publications not included in this thesis

I. **The role of Pd-Pt interactions in the oxidation and sulfur resistance of bimetallic Pd-Pt/γ-Al₂O₃ diesel oxidation catalysts**

Phuoc Hoang Ho, Jung-Won Woo, Rojin Feizie Ilmasani, Joonsoo Han, Louise Olsson
Industrial & Engineering Chemistry Research 2021, 60, 6596-6612.
<https://doi.org/10.1021/acs.iecr.0c05622>

II. **Chemical poisoning by zinc and phosphorous of Pt/Ba/Al₂O₃ NO_x storage catalysts**

Rasmus Jonsson, Rojin Feizie Ilmasani, Torben Nilsson Pingel, Magnus Skoglundh, Eva Olsson, Malin Berggrund, Louise Olsson
Applied Catalysis A: General 2019, 571, 158-169. <https://doi.org/10.1016/j.apcata.2018.11.027>

Contribution Report

Paper I

The author synthesized the catalyst samples, performed the catalyst characterizations (except for STEM/EDX and ICP-SFMS), conducted the flow reactor experiments, interpreted the results together with the co-authors and was responsible for writing the manuscript.

Paper II

The author synthesized the catalyst samples, performed the catalyst characterizations (apart from STEM/EDX, XPS and ICP-SEMS), conducted the flow reactor experiments, interpreted the results together with the co-authors and was responsible for writing the manuscript.

Paper III

The author synthesized the catalyst samples, conducted the flow reactor experiments and characterization tests (except for ESEM-EDX, XPS and ICP-SEMS) and interpreted the experimental results together with the co-authors.

Paper IV

The author synthesized the catalyst samples, conducted the flow reactor experiments and characterization tests (aside from STEM, DRIFTS and ICP-SEMS) and interpreted the experimental results together with the co-authors.

Paper V

The author synthesized the catalyst samples, performed the catalyst characterizations (except for SEM/EDX, XPS, NMR and ICP-SEMS), conducted the flow reactor experiments, interpreted the results together with the co-authors and was responsible for writing the manuscript.

Abbreviations

AFR	Air to Fuel Ratio
BET	Brunauer-Emmet-Teller
CEM	Controlled Evaporator and Mixer
DRIFTS	Diffuse Reflectance Infrared Fourier Transform Spectroscopy
EDX	Energy Dispersive X-ray
ESEM	Environmental Scanning Electron Microscope
FTIR	Fourier Transform Infrared Spectroscopy
HC	Hydrocarbon
ICP-SFMS	Inductively Coupled Plasma Sector Field Mass Spectrometry
LNT	Lean NO _x Trap
MFC	Mass Flow Controller
MS	Mass Spectrometer
NMR	Nuclear Magnetic Resonance
PNA	Passive NO _x Adsorber
SAR	Silica to Alumina Ratio (molar ratio SiO ₂ /Al ₂ O ₃)
SCR	Selective Catalytic Reduction
STEM	Scanning Transmission Electron Microscopy
TEM	Transmission Electron Microscopy
TPD	Temperature Programmed Desorption
TPO	Temperature Programmed Oxidation
TPR	Temperature Programmed Reduction
XPS	X-ray Photoelectron Spectroscopy
XRD	X-ray Powder Diffraction

Contents

1	Introduction.....	1
1.1	Emission control.....	1
1.2	NO _x reduction technologies.....	2
1.3	Objectives.....	3
2	Passive NO _x adsorber.....	5
2.1	Key factors in PNAs.....	5
2.2	NO adsorption and desorption.....	6
2.2.1	Exhaust species.....	8
2.2.2	Promoters.....	9
2.2.3	Hydrothermal aging and pretreatment.....	9
2.2.4	Phosphorous and sulphur poisoning.....	10
3	Experiments and equipment.....	11
3.1	Sample synthesis.....	11
3.1.1	Pd/zeolites.....	11
3.1.2	SSZ-13 synthesis.....	12
3.1.3	Modified 1%Pd/zeolites.....	12
3.1.4	Monolith preparation.....	15
3.2	Flow reactor and NO adsorption/desorption activity.....	15
3.3	Characterisation techniques.....	18
3.3.1	Inductively coupled plasma sector field mass spectrometry (ICP-SFMS).....	18
3.3.2	Specific surface area analysis (BET).....	18
3.3.3	Scanning transmission electron microscopy (STEM).....	19
3.3.4	Environmental scanning electron microscope (ESEM).....	19
3.3.5	Energy dispersive X-ray (EDX).....	19
3.3.6	X-ray photoelectron spectroscopy (XPS).....	20
3.3.7	X-ray powder diffraction (XRD).....	20
3.3.8	Temperature programmed oxidation (TPO) and reduction (TPR).....	21
3.3.9	Solid state nuclear magnetic resonance (NMR).....	22
3.3.10	<i>In-situ</i> DRIFT spectroscopy.....	22
4.	Palladium supported on modified beta zeolite.....	25
4.1	PNA activity tests.....	25

4.1.1	Study of different promoters on Pd/BEA and hydrogen pretreatment effects	25
4.1.2	Various La loadings and the effect of H ₂ O.....	27
4.1.3	Effect of CO on the sequential passive adsorption of NO _x	29
4.2	Physicochemical characterisation.....	32
4.3	DRIFT spectroscopy.....	36
5.	Assisting and degrading behaviour of CO in PNAs	39
5.1	Characterisation of the synthesised Pd/SSZ-13.....	39
5.2	PNA activity tests	40
5.2.1	Effect of CO on the passive adsorption of NO _x	40
5.2.2	Degrading effect of CO on the passive adsorption of NO _x	44
5.3	Physicochemical characterisation.....	46
6.	The Effect of phosphorous poisoning on PNAs	49
6.1	Characterisation of the synthesized Pd/SSZ-13.....	49
6.2	Physicochemical characterisation.....	50
6.3	DRIFT spectroscopy.....	52
6.4	PNA activity tests	54
7.	Conclusions and outlook.....	57
	Acknowledgements	61
	References	63

Chapter 1

1 Introduction

1.1 Emission control

Fulfilling the needs of modern society requires the conversion of sufficient amounts of energy for transportation, heating and industry. The exhaust gases created by these activities can contain air pollutants that can affect both the local and global environments negatively¹⁻². In addition to air pollution, the CO₂ formed during combustion contributes to global warming, confirming that the use of renewable energy sources is of utmost importance. The main air pollutant compounds are carbon monoxide (CO), nitrous oxides (NO_x), sulphur oxides (SO_x), hydrocarbons (HC) and particulate matters (PM). The transportation sector, which has been growing rapidly since the 1970s, was the second largest contributor after the power generation sector of greenhouse gas emissions in 2015²⁻⁵. Consequently, lean-burn gasoline and diesel engines were introduced to increase fuel efficiency and decrease emissions⁶. Such engines use a higher air-to-fuel ratio (AFR) than Otto engines, resulting in more efficient combustion due to the fuel being utilised to a greater extent⁷. Although the lean-burn combustion concept is beneficial to the improvement of fuel economy, NO_x reduction over a three-way (TWC) catalyst to N₂ in an oxygen-rich environment is not, however, possible⁸⁻⁹. NO_x emissions are harmful and toxic, and can cause environmental, ecological and health issues¹⁰⁻¹¹. The strict regulations placed on emissions of nitrogen oxides (NO_x)¹² make the

development of an effective and economical catalyst system that can control NO_x emissions in lean exhaust stream necessary.

1.2 NO_x reduction technologies

Nitrogen oxides (NO_x) is a general term for NO and NO₂ both of which are highly reactive and poisonous gases. NO_x emissions can react in the atmosphere to form ozone (O₃), acidic rain and smog^{10,13}. NO_x can form in diesel engines in several ways: when the temperature in the combustion chamber exceeds 2000 K (thermal NO_x), via oxidation of already ionized nitrogen compounds in the fuel (fuel NO_x) and from a combination of nitrogen molecules in the air with fuel (prompt NO_x)¹⁴.

Selective catalytic reduction (SCR) and lean NO_x traps (LNT) are techniques commonly applied after lean-burn engines to achieve high levels of efficiency in reducing NO_x emissions¹⁵⁻¹⁶. However, both methods have their own limitations in cold-start conditions. In the case of SCR systems, a continuous selective catalytic reduction of NO_x to N₂ and H₂O occurs via a reaction with NH₃ originating from urea. Being in the liquid form, urea must first be decomposed and hydrolysed to form NH₃, which requires high temperatures (> ~200°C). One of the present limitations of SCR is the very low rate of decomposition of urea¹⁷⁻¹⁸ at both low engine operating temperatures (<200°C) and during cold-starts; the large amount of biproducts that are formed means that injections of urea are not possible. On the other hand, LNT, using lean/rich cycles (oxygen excess/fuel excess), has been introduced in which NO_x is trapped under lean conditions in the form of nitrates and nitrites on a storage compound; the catalyst is regenerated following saturation of the storage compound (under rich conditions)¹⁹⁻²⁰. However, low temperature operating conditions lower the efficiency of oxidizing NO to NO₂²¹⁻²², thereby reducing the trapping efficiency of NO_x. Furthermore, regeneration of the stored NO_x is limited at low temperature.

Multiple adsorbents, with the ability of temporarily storing NO_x at low temperature and then releasing it by increasing the temperature, have been examined in the quest to control NO_x emitted during cold-start. Known as passive NO_x adsorbers (PNA), these are intended to be located upstream of an SCR catalyst. NO_x is adsorbed at low temperatures and then desorbed once the temperature of the engine has been increased. The goal is that the NO_x release occurs at a temperature above ~200°C (the temperature of urea dosing) in order to facilitate its removal in the SCR system. Although many studies have confirmed that noble metals (Pd, Pt and Ag) supported on alumina/ceria are promising adsorbents^{17, 23-24}, these adsorbents show a high tendency of being afflicted by sulphur poisoning and has resulted in

great interest being directed towards materials with zeolite supports and, most often, Pd as the noble metal^{22, 25}. Pd/zeolite adsorbents have a high adsorption capacity, but the desorption temperatures can still be modified by promoters. Studies of PNA applications have shown that low levels of CO affect the activity of the adsorbent beneficially with respect to both the amount of NO_x that can be stored and the temperature of the NO_x release²⁶. However, recent studies have revealed that the presence of high levels of CO during long-term sequential NO_x adsorption and desorption deactivates the Pd/zeolite material severely²⁷⁻²⁸. According to different studies, phosphorous is also known to be an element causing severe deactivation in both NH₃-SCR and PNA catalytic systems²⁹⁻³².

1.3 Objectives

The fundamental objective of this thesis was to provide a deeper understanding of PNA processes and the effect of various conditions on the performance of Pd/zeolite-based adsorbents. More specifically, the study started with the effect of different promoters on 1%Pd/BEA zeolite (SAR of 38). Thereafter, the behaviour of the La-promoted sample led to the further study of various concentrations of lanthanum on the PNA process, as reported in **Paper I**. In **Paper II** the performance of a La-promoted Pd/BEA sample for multiple NO_x adsorption/desorption cycles in the presence of a high concentration CO was investigated. The focus of **Papers III** and **IV** was placed on gaining a deeper understanding of the effects of low and high concentrations of CO on the performance of Pd/SSZ-13 during multiple cycles; detailed reaction mechanisms were proposed regarding these experimental conditions. The study presented in **Paper V** concentrated on the degrading effect of phosphorus on Pd/SSZ-13 in the adsorption and desorption steps. Various characterisation techniques, combined with a flow reactor setup, were used in order to comprehend the effects of different factors on the Pd/zeolite adsorbent in the PNA processes investigated in the papers.

Chapter 2

2 Passive NO_x adsorber

Passive NO_x adsorber in after-treatment systems of diesel engines are designed to adsorb NO_x emitted during cold-start periods. A cold-start period can generally be referred to as the very first time an engine starts operating after a long continuous shut-down, and ends when the catalyst has reached its operating temperature. PNA is thus of interest, since it can store the NO_x generated at low temperature during a cold-start³³. The engine's temperature eventually exceeds 180-200°C (the minimum urea dosing temperature), which is when NO_x reduction catalysts can begin to operate efficiently. The adsorber should therefore ideally begin to release NO_x after 200°C has been reached. However, the temperature should not be too high, since there is then a risk that PNA will not be regenerated properly.

2.1 Key factors in PNAs

There are three factors that are important for an adsorbent in PNA processes: storage capacity of NO_x at low temperatures, desorption temperature and degradation resistance. The storage at a certain temperature can be calculated by the amount of NO_x adsorbed per unit mass of the adsorbent³⁴. Greater NO_x adsorption at low temperatures is generally more desirable to ensure efficient performance and to minimise the amount of adsorbent required for trapping cold-start NO_x. The desorption temperature is referred to as the temperature at which the adsorbed NO_x begins to be released whilst the catalyst is heating up.

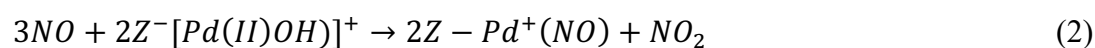
The desorption temperature range can vary for different materials: ideally, desorption should not begin until 200°C has been reached and be complete by the time 400°C has been reached^{25, 33, 35-38}. Degradation occurs for PNAs due to several thermal aging and poisoning conditions. Such degradation can appear either as a lowering of the NO_x storage capacity, coupled with a corresponding lowering in the amount of desorption, or result in a shift of the adsorption/desorption temperatures to non-optimal ranges. Degradation can be a crucial factor that affects the lifetime of the PNA, so monitoring the deactivation that can occur during PNA experiments is therefore of importance.

2.2 NO adsorption and desorption

NO_x produced at low temperatures is usually in the form of NO in the exhaust gases, making the adsorption of NO the focus of PNAs. Supported precious metals, such as Pt, Pd and Ag, are the materials most studied as adsorbents in PNA processes^{17, 22-23, 25, 34, 39}. Crocker *et al.*, who studied alumina and ceria base materials with Pt and Pd, found a superior NO_x adsorption performance when Pt and Pd were present in the adsorbents^{17, 24, 40}. In another study, Chen *et al.* showed that, with various loadings of Pt and Pd, the NO_x was stored significantly at low temperatures in Pt/Pd/CeO₂³⁴. According to a study by Ryou *et al.*, Pd/CeO₂ performed better than Pt/CeO₂ and Pt/Pd/CeO₂ based PNAs³⁸. However, later reports in the literature have shown that these materials can undergo severe degradation in NO_x storage capacity due to sulphur poisoning^{22-23, 41}.

Consequently, attention was turned to the use of zeolite based materials. Chang *et al.* assessed the performance of Ca/beta zeolites and showed an increase in NO_x trapping with this material. They also reported that, when increasing the loading of CaO from 5 to 10 wt.%, the penetration time (time required for NO to be detected in the reactor outlet during adsorption) increased from 38 to 51 min⁴². Chen *et al.* reported that the NO_x storage capacity of Pd/BEA, Pd/MFI and Pd/CHA remained almost the same even after exposure to 21 mol of SO₂ per mole of Pd at 100°C²². Many other studies have been carried out in more detail regarding Pd-based zeolites and, as an example, Pd/BEA, all of which showed a significant storage capacity in PNA experiments^{25-26, 43-44}. Therefore, it appears that Pd has become the preferred precious metals for PNAs: the highest NO_x storage was achieved for loadings of ~1 wt.% Pd^{22,26}. Concentrations exceeding 1 wt.% for Pd limits the dispersion of Pd cations, and it is critical that high levels of ion-exchange are achieved.

Pd particles on zeolite supports in PNA processes can be in different forms, such as clusters, nanoparticles and ion-exchanged metal sites^{25, 45-47}. Pd clusters and particles are larger than the pore size of zeolite support and are therefore easily detected on the surface of the support²⁵. Ion-exchange Pd sites result from an interaction of Pd atoms and Brønsted acid sites that can form between a proton in acid sites and a metal cation⁴⁸. The NO adsorption sites were found to be mainly the ion-exchanged Pd cations in the zeolite framework²². Pd in these sites can be bonded with either two Al and form $Z^-Pd^{2+}Z^-$ or one Al and one OH group and form $Z^- [Pd(II)OH]^+$. Palladium can also be present as PdO_x clusters on the zeolite surface^{47, 49-50}. According to Zheng *et al.*²⁵, the trapping and release of NO_x entails complex adsorption and desorption processes involving complicated chemical reactions. The simplified reactions below are suggested for trapping NO under dry conditions²⁵:



where Z^- is a cationic exchange site.

In this case, Pd(IV) can be reduced to Pd(II) during NO adsorption, and the Pd(II) formed can then become another adsorption site. In addition, Zheng *et al.* also reported that the ability of NO_x to adsorb on Pd(IV) declines in the presence of water²⁵. Moreover, results from Chen *et al.* showed that hydrothermal aging caused the PdO particles to transform into ionic Pd, which increased the NO_x storage capacity of Pd/zeolite base materials³⁵. It has thus been found that ionic Pd²⁺ particles are the main NO_x adsorption sites at low temperatures in the presence of water²².

In research studies it is common that, following isothermal NO_x storage, temperature-programmed desorption is applied to investigate the desorption properties of the adsorbent. The desorption process should start at a temperature at which the downstream NO_x reduction catalyst is active. In the case of NH₃-SCR systems, the minimum desorption temperature required is about 200°C^{16, 51}. Desorption at too low a temperature causes the ineffective NO_x reduction and, conversely, too high a temperature can inhibit the regeneration or removal of NO_x for future cycles^{26, 52}. Many of the important factors that can affect the adsorption and desorption properties of PNA processes are listed in Sections 2.2.1-2.2.4.

2.2.1 Exhaust species

Exhaust from lean-burn engines generally contains many species aside from NO_x. These additional species include O₂, N₂, CO, H₂O, hydrocarbons, SO₂ and CO₂. N₂ has no effect on the adsorption and desorption of NO_x due to its inert properties. It has been reported by Khivantsev *et al.* that oxygen can have an effect in PNA, and specially in Pd-zeolite adsorbents, by activating an extra NO adsorption bond resulting from the generation of nitrates⁴⁷. The presence of CO₂ has been shown to have a negative impact on the NO_x adsorption of non-zeolite based adsorbents, which can be due to the formation of carbonates and their competition with NO_x for adsorption sites²⁴. According to Mihai *et al.* and Vu *et al.*, however, CO₂ has no effect on the adsorption of NO_x on Pt/Pd supported on zeolites^{26, 53}.

The effect of H₂O has been studied in many papers. All results show that water severely diminishes NO_x storage at low temperatures, due to blockage not only of Brønsted acid sites by H₂O molecules^{21,25,54-55} but also of the Lewis acid sites, such as Pd. Correspondingly, lower NO_x adsorption in the presence of water leads to lower desorption as well. Theis *et al.* showed that the presence of water suppressed the NO_x trapping capacity at low temperatures (<100°C) for both Pd and Pt on Al₂O₃ or CZO (ceria zirconia mixed oxide). This was due to the condensation of water on the storage sites⁵⁶.

Various studies indicated that CO could improve the NO_x storage capacity and reduce the negative effects of H₂O either by Pd reduction or by formation of nitrogen-carbon-oxygen species^{25, 55-56}. Vu *et al.* examined the effect of different concentrations of CO (from 0-225 ppm) and it was observed that by increasing the quantity of CO larger NO_x desorption could be achieved for Pd/BEA²⁶. Also it was observed that the desorption peaks at low temperatures (<200°C) for Pd/BEA were shifted to higher temperatures with CO due to more stable Pd oxidation states²⁶. This is a beneficial effect for PNA processes for the cases where the desorption was at temperatures below urea dosing. In addition, it was also reported that at higher temperatures (>200°C) the release peak shifted to lower values (still higher than 200°C)⁵⁵. Some studies claimed that the co-adsorption of NO and CO on palladium sites, forms more stable bonds or the reduced Pd species with CO were more efficient in NO adsorption^{25, 35, 57}. However, no agreement on the precise mechanism of the CO effect has been reached in the previous studies.

It is important to mention that for vehicle engines, there can be multiple cold-start steps, thus it is important to know how the PNAs behaviour will be after several NO_x adsorption/desorption cycles. Recent studies by Yuntao *et al.* and Theis *et al.* indicated that repeated NO_x storage and release cycles with a high CO concentration can cause a gradual

degradation of the NO_x adsorption and desorption over Pd/Zeolite materials²⁷⁻²⁸. It has been reported that a high concentration of CO causes Pd sintering, which can be a reason why the adsorbents degrade in multiple cycles²⁸. However, no precise sintering mechanism has been reported, and no adsorbent that may be resistant or less sensitive to the CO degradation mechanism has been identified.

2.2.2 Promoters

A few studies have been made on the addition of promoters to PNA systems. Ji *et al.*²⁴, who studied the performance of La-promoted Pt/Al₂O₃ in PNA processes whilst also varying the concentrations of La on the adsorbent, found that the presence of La enhanced the formation of nitrate bonds²⁴. In another study, where Crocket *et al.* investigated different promoters for Pt/Pd/metal oxide, it was mentioned that the lanthanum group of metals showed a beneficial behaviour towards Pt/Pd/metal oxide materials in PNA processes⁴⁰. Jones *et al.* examined the effects of various promoters, too, including those of La group metals on Pt/CeO₂ and Pd/CeO₂ and reported that Pr had a positive effect as a promoter in both the adsorption and desorption of NO_x¹⁷. However, to the best of this author's knowledge, our studies are the first that examine the effects of promoters on Pd/zeolites.

2.2.3 Hydrothermal aging and pretreatment

Ryou *et al.* showed that the hydrothermal aging (HTA) of Pd/SSZ-13 enhanced the storage performance of NO at low temperatures. They found that HTA was helpful in the range 700-750°C but that temperatures over 850°C caused the Pd particles to agglomerate, which reduced the storage capacity. According to H₂-TPR, they claimed that this enhancement by HTA is due to an increased distribution of PdO into highly dispersed Pd²⁺ species within the zeolite structure³⁵⁻³⁶. This was also reported by Okumura *et al.* for Pd supported on ZSM-5⁵⁸.

In many research studies, a pretreatment step precedes the NO_x storage and release steps in order to ensure complete removal of all NO_x residuals from the adsorbent. The pretreatment step can consist of a reducing agent, such as H₂, along with O₂ and H₂O at high temperature. The pretreatment step with hydrogen can have an important effect on the nature of the Pd oxidation state⁴⁵. At sub-ambient temperatures, hydrogen can reduce PdO_x particles and also form PdH⁵⁹⁻⁶⁰ and, at higher temperatures, Pd ionic species can become reduced to lower oxidation states^{45, 48, 61}. In another study, increased mobility of reduced Pd species was

observed, which can lead to Pd agglomeration on the surface⁴⁸. H₂ pretreatment can therefore have undesirable effects on PNAs that contain Pd.

2.2.4 Phosphorous and sulphur poisoning

One of the most common deactivation processes prevalent in exhaust aftertreatment catalytic systems is chemical poisoning and this is often originating from sulphur and phosphorus.

Sulphur can cause chemical poisoning in automotive catalytic systems^{41,62} originating from fuel, that combined with oxygen to form SO₃ leading to formation of sulphates and sulphuric acid, that block the surface and causing deactivation of the catalysts⁶³⁻⁶⁴.

Phosphorus mostly originates from lubricant oils such as zinc dialkyldithiophosphates (ZDDP) or biomass-based fuels⁶⁵⁻⁶⁶. Its high stability can cause difficulties in the regeneration of the catalyst, which makes the presence of phosphorous one of the most serious poisoning conditions in catalytic systems^{65, 67}. Many studies have shown that phosphorous deactivates NH₃-SCR catalysts^{30-31, 68}. This deactivation was due to the loss of active sites, which was caused by blockage or interaction with phosphorous, and the dealumination and destruction of the zeolite framework^{30, 32}. It was reported that Pd-Pt/Al₂O₃ is poisoned after exposure to phosphorous⁶⁹. Xie *et al.* showed that metaphosphates were the main phosphorous species formed on Cu/SSZ-13³⁰. Moreover, Chen *et al.* recently reported formation of metaphosphates as a dominant P-compound after poisoning of Pd/zeolite in PNA processes²⁹. Studies on the effect of hydrothermal aging on P-poisoned zeolites have illustrated the destruction of zeolite through the formation of the AlPO₄^{68, 70}. Wang *et al.* claimed that the interaction of phosphorous species with Cu²⁺ and Cu²⁺OH sites in Cu/SSZ-13 caused degradation of the catalyst activity³¹.

Chapter 3

3 Experiments and equipment

The performance and stability of PNA adsorbents were investigated in flow reactor experiments and followed by detailed characterisations in order to improve understanding of the reactor results. The characterisation methods used were BET, STEM, XPS, TPO, O₂-TPD, SEM EDX mapping, XRD, NMR and *in-situ* DRIFTS analysis. The synthesis of the samples and the characterisation methods are described in the following sections.

3.1 Sample synthesis

3.1.1 Pd/zeolites

In all samples, Pd was used with zeolite supports (beta and SSZ-13) and deposited by means of an “incipient wetness impregnation” method on the support material. The reference sample in **Papers I** and **II** was Pd/BEA, which consisted of 1 wt.% Pd loaded on a beta zeolite support. Several reference samples were prepared using a diluted Pd precursor solution of palladium (II) nitrate (4-5 wt.% Pd) from Sigma-Aldrich and commercial beta zeolite (CP814C, SAR (SiO₂-to-Al₂O₃ molar ratio 38) from Zeolyst International. In **Paper I**, the PNA synthesis began with promoters (Section 3.1.2) followed by impregnation of Pd on the promoted beta support. Thereafter, in **Paper II**, the promoted sample was prepared in a reverse sequence. Pd/SSZ-13 was used as the adsorbent material with 1 wt.% Pd (palladium (II) nitrate, Sigma-Aldrich and 4-5 wt.% Pd) loading on SSZ-13 in **Papers III-V**.

3.1.2 SSZ-13 synthesis

For **Papers III-V**, the SSZ-13 zeolite support was synthesized using the hydrothermal method⁷¹⁻⁷³, with SAR (SiO₂-to-Al₂O₃ molar ratio) of around 12. Firstly, 0.8 g of NaOH (Sigma-Aldrich, >98 %) was dissolved in 66 g deionized (D.I) water, followed an addition of 18 g SDA (TMAda-OH, Sigma-Aldrich) and 1.38 g Al(OH)₃ (Sigma-Aldrich) under stirring. 12 g of fumed silica (Sigma-Aldrich), with an average particle size of 7 nm, was then added gradually to the solution while being stirred vigorously in order to achieve a fully homogenized gel. The gel thus prepared was sealed in two Teflon-lined 75 ml autoclaves with constant stirring at 160°C for 96 h. After hydrothermal synthesis, the autoclaves were cooled at room temperature and washed 10 times with D.I. water until an appropriate pH value (below 8) was reached. The final solid was dried overnight at 85°C and then calcined at 600°C for 8 h to obtain Na-SSZ-13. In **Paper V**, an ion-exchange procedure was performed by mixing the powder with 43.2 g NH₄NO₃ (99%, Sigma-Aldrich) in 100 ml D.I. water at 80°C for 15 h to produce NH₄/SSZ-13⁶². This step was done twice to make certain that the Na⁺ cations were exchanged to NH₄⁺ to a sufficiently high extent (Na concentration >0.05 wt.%). The ion exchange step in **Papers III and IV** was conducted at 80°C for 2 h instead of 15 h. The zeolite synthesis was finalised by drying the ion-exchanged powder overnight at 85°C, followed by calcination at 550°C for 4 h to remove NH₄⁺ and produce H-SSZ-13 which was used to load Pd.

Incipient impregnation method

The preparation of the samples by this method required a corresponding amount of Pd(NO₃)₂ solution (for 1 wt.% loading) to be diluted in a specific amount of MilliQ water (Millipore): the amount of water is related to the total pore volume of the support material. The solution was added dropwise to the support material and fully mixed with a spatula. The resulting powder was dried overnight at 100°C and followed by calcination at 500°C for 5 h, using a temperature ramping rate of 2°C/min.

3.1.3 Modified 1%Pd/zeolites

The promoters studied in **Paper I** were comprised of ceria (Ce), zirconium (Zr) and lanthanum (La), with loadings of 10 wt.%. The commercial precursors used, all from Sigma-Aldrich, were cerium (III) nitrate hexahydrate, zirconium (IV) oxynitrate hydrate and lanthanum (III) nitrate hydrate, respectively. Preparation of these three samples involved the promoters first being impregnated on the beta zeolite, before Pd was loaded on the promoted

support. The target loading concentration of the promoters (10 wt.%) was achieved in two steps of 5 wt.% depositions, using an incipient wetness impregnation method. After each loading step, the powder was dried overnight at 100°C and finally, after reaching 10 wt.% loading of the promoter, calcination at 500°C for 5 h followed the drying step. The promoted zeolite was thereafter impregnated with the Pd solution to reach 1 wt.% loading, dried further and calcined in the same manner. Moreover, in **Paper I** different concentrations of La were studied ranging from 2.7 to 10 wt.%. The synthesis of these samples started with a large batch of 2.7 wt.% La loaded on the zeolite support. After drying overnight, higher concentrations of La were loaded gradually in steps, with the sample being dried at 100°C overnight between each one. Samples with 2.7, 3.5, 5.4, 7.0 and 10.0 wt.% La were calcined at 500°C for 5 h, following a temperature ramp of 2°C/min. 1 wt.% Pd was eventually deposited on the promoted zeolite samples.

Three main samples were studied in **Paper II**, namely 1 wt.%Pd/BEA, used as a reference sample, and two La-promoted samples (2.7wt.% La): one with and one without palladium. Another sample of La-modified Pd/BEA was also synthesized, using a reverse loading sequence. These samples were prepared employing the same incipient wetness method as before. All of the samples prepared are listed in Tables 1 and 2, and are named respective to the loading sequence of metals on the BEA zeolite: in the case of 2.7%La-Pd/BEA, for example, La was loaded on the support before Pd.

Table 1. List of samples prepared in **Paper I**.

Adsorbent Material	Metal Loading (wt.%) ¹			
	Pd	Ce	Zr	La
10%Ce-Pd/BEA	0.9	10.0	-	-
10%Zr-Pd/BEA	0.9	-	10.0	-
10%La-Pd/BEA	1.0	-	-	10.0
7%La-Pd/BEA	0.9	-	-	7.0
5.4%La-Pd/BEA	0.9	-	-	5.4
3.5%La-Pd/BEA	1.0	-	-	3.5
2.7%La-Pd/BEA	0.9	-	-	2.7
Pd/BEA	0.9	-	-	-

¹ Specified loadings are based on ICP-SFMS analysis of the adsorbent materials prepared.

Table 2. List of samples prepared in **Paper II**.

Adsorbent Material	Metal Loading (wt.%) ¹	
	Pd	La
2.7%La-Pd/BEA	0.9	2.7
Pd-2.7%La/BEA	1.1	2.7
Pd/BEA	1.1	-
2.7%La/BEA	-	2.7

¹ Specified loadings are based on ICP-SFMS analysis of the adsorbent materials prepared.

1 wt.% Pd/SSZ-13 was used in **Papers III** and **IV** for the various NO-TPD experiments. In **Paper V** three different phosphorous loadings were studied on Pd/SSZ-13 and compared with the non-poisoned Pd/SSZ-13. As mentioned earlier, Pd/SSZ-13 can adsorb larger amounts of NO_x after hydrothermal aging at 750°C, due to more Pd²⁺ species being created by the transformation of Pd clusters³⁵. It is nevertheless known that the hydrothermal aging of phosphorous-poisoned Cu/SSZ-13 causes the destruction of the zeolite⁶⁸. Degreening was therefore carried out in this work, prior to phosphorous loading. The Pd/SSZ-13 powder was first degreened at 750°C for 1h, using 400 ppm NO, 8% O₂ and 5% H₂O, in a crucible placed in the flow reactor. Thereafter, the incipient impregnation method was employed to load an aqueous (NH₄)₂HPO₄ solution on the degreened Pd/SSZ-13 sample to reach the target value of the phosphorous loading. The samples were subsequently dried overnight at 85°C before being calcined at 550°C for 4 h with a temperature ramping rate of 2°C/min. Three different concentrations of phosphorous-poisoned Pd/SSZ-13 were prepared: 0.4, 0.6 and 0.8 mmol g⁻¹. The synthesis of these samples started with a large batch of 0.4 mmol g⁻¹ phosphorous loaded on the zeolite support. After drying overnight, higher concentrations were prepared by increasing the phosphorous loading for part of the initial 0.4 mmol g⁻¹ batch, prior to drying overnight and calcining at 550°C for 4 h. The P-poisoned samples prepared were denoted as 0.4P, 0.6P and 0.8P, respectively, in this paper. Table 3 lists all of the samples prepared in **Papers III-V**.

Table 3. List of samples prepared in **Papers III-V**.

Adsorbent Material	Metal Loading (wt.%) ¹	
	Pd	P
Pd/SSZ-13 (Paper III)	0.98	-
Pd/SSZ-13 (Paper IV)	0.98	-
Pd/SSZ-13 (Paper V)	1.1	-
Pd/SSZ-0.4P (Paper V)	1.0	1.3
Pd/SSZ-0.6P (Paper V)	1.04	1.5
Pd/SSZ-0.8P (Paper V)	1.1	2.6

¹ Specified loadings are based on ICP-SFMS analysis of the adsorbent materials prepared.

3.1.4 Monolith preparation

The samples were washcoated onto honeycomb-structured cordierite monoliths (cpsi: 400) for flow reactor measurements. All monoliths were cut to a length of 2 cm and diameter of 2.1 cm before being heated at 550°C for 2 h in air to remove contaminants. The slurry prepared for coating had a 90:10 mass ratio of liquid to solid phase. The solid phase contained the powder sample and boehmite binder (Dispersal P2), with a mass ratio of 95:5, and the liquid phase contained a 50:50 mass ratio of water and ethanol. These values were the same in all five papers. The monoliths were coated by droplets of the solid/liquid solutions and dried at 90°C for 2 minutes with a heating gun. This was repeated several times until the desired loading of washcoat was reached (~700 mg). Finally, the prepared monoliths were calcined at 500°C for 2 minutes with a heat gun, and then calcined for 2 hours at 500°C in a calcination oven.

3.2 Flow reactor and NO adsorption/desorption activity

Continuous gas flow reactor studies were used to examine PNA activity under different operating conditions. The coated monoliths were inserted in a horizontal quartz tube in the reactor experiments: they were all first wrapped with quartz wool to prevent gases from bypassing the channels. The tube was then placed in a heating coil and covered with insulating material. Two type-K thermocouples were passed through the coated monoliths from the downstream end for temperature measurements: one was placed with its tip located ca. 2 cm upstream of the monolith to measure the inlet gas temperature, and the other was placed ca. 0.5 cm inside the monolith to register the temperature of the sample. Fig. 1 shows a schematic diagram of the experimental setup of the flow reactor. Bronkhorst mass flow controllers (MFC)

were used for regulating and controlling the inlet gases whilst the feed rate of the water was regulated by a controlled evaporation and mixing (CEM) device. An MKS Multi-Gas 2030 HS FTIR spectrometer was used to monitor the outlet gases. The total gas flow rate during the TPD experiments was 750 ml min^{-1} in **Papers I-IV**, whereas a total flow of 550 ml min^{-1} was used in **Paper V**; it was changed to 750 ml min^{-1} in one of the cycles to study the effect of the flow rate.

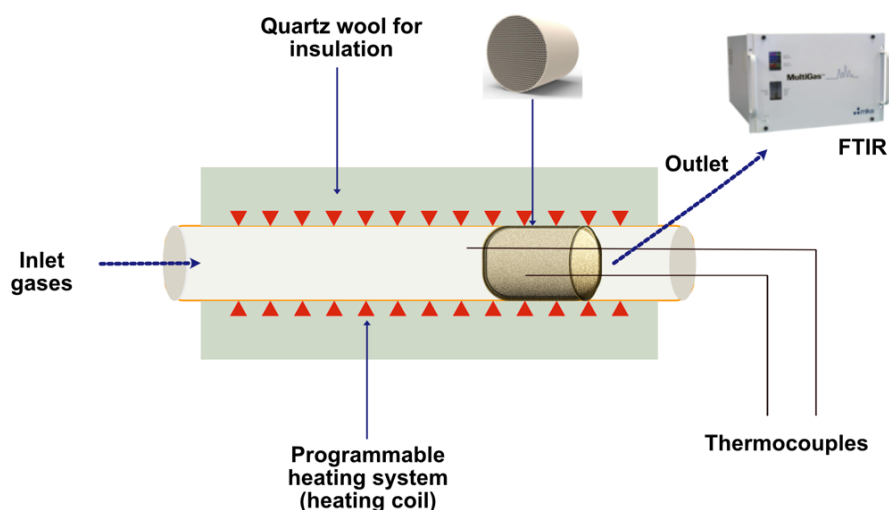


Figure 1. Schematic diagram of the used flow reactor, inspired by Azis and Yao et al.^{49, 74}.

In studies **I** and **II**, a degreening step was performed at the beginning of the experiments with 1h exposure to 500 ppm NO, 8% O₂ and 5% H₂O at 750°C and an argon balance, at the rate of 20 °C/min. The same degreening step was performed in **Papers III-V** except that the inlet gas was comprised of 400 ppm NO.

In **Paper I**, the degreening step was followed by a pretreatment step at 650°C for 15 min in 1% H₂ and 5% H₂O, with an Ar balance. This pretreatment was used in the performance studies of different promoters. The effect of hydrogen pretreatment was also studied in the TPD by comparing two different pretreatment conditions: (i) 1% H₂ and 5% H₂O, with an Ar balance, for 15 minutes at 650°C and (ii) only Ar flushing for 15 minutes at 750°C. The study continued by cooling the pretreatment temperature down from 650°C to 80°C (the adsorption temperature) under the conditions of 8% O₂, 5% H₂O and Ar. The storage step comprised of 200 ppm NO, 8% O₂, 5% H₂O and Ar at 80°C for 45 min. The desorption step started by ramping up to 650°C at a rate of 20 °C/min, with the same gas composition as the storage step. In this study, the water effect was also studied in the same reactor experiment but with water absent from the gas composition, and denoted as “dry conditions” (**Paper I**).

All samples in **Paper II** were exposed to 10 cycles of NO_x adsorption/desorption after the degreening and pretreatment steps. The storage step consisted of 200 ppm NO, 4000 ppm CO, 8% O₂, 5% H₂O and Ar at 80°C for 45 min. The temperature was increased thereafter to 500°C, at a rate of 20 °C/min, for NO_x desorption with the same feed gas mixture. Prior to each cycle, a pretreatment step was applied at 500°C with 8% O₂, 5% H₂O and Ar for 15 min.

Multiple NO-TPD cycles were performed in **Paper III**; prior to all of the cycles, the adsorbent was degreened at 750°C for 1h in 400 ppm NO, 8% O₂ and 5% H₂O, and pretreated at 550°C for 30 min with 8% O₂ and 5% H₂O. Cycle 1 was an adsorption step at 80°C for 45 min in a gas mixture of 200 ppm NO_x, 8% O₂ and 5% H₂O in Ar balance, followed by a desorption step whilst simultaneously being ramped up to 550°C at a rate of 20 °C/min in the same gas mixture. Cycle 2 was repeated with the same inlet adsorption and desorption conditions as Cycle 1 in order to investigate the reproducibility of the adsorption of NO_x. The NO inlet concentration in Cycles 3-4 and 5-6 was set to 300 and 400 ppm, respectively. The final cycle had the same conditions as Cycles 1 and 2 to check the stability of the adsorbent: A small amount of NO₂, with the molar proportion of NO₂/NO_x=1.8 mol%, had been available in the inlet feed gas while NO was being injected into the system. In the second part of the PNA experiment in this paper, the effect of various CO concentrations was studied. While retaining the inlet NO concentration at 200 ppm, the CO concentration was set to 200 ppm in Cycles 1-2 and 400 ppm in Cycles 3-4. Cycle 5 was the same as Cycles 1-2 so that the stability of the adsorbent could be investigated. The same experiments were performed in an empty reactor, as a step test to be used as the inlet condition for the kinetic modelling.

In **Paper IV**, the adsorbents were exposed to the same degreening conditions as in **Paper III** in order to achieve higher quantities of Pd²⁺ and stabilise the Pd species⁷⁵. In this paper, 15 cycles of NO-TPD were conducted. The inlet gases of the first two cycles had 200 ppm NO, 8% O₂ and 5% H₂O in Ar balance; in the remaining cycles, 4000 ppm CO was added to the inlet gases. The same experiments were performed in an empty reactor, as a step test to be used as the inlet condition for the kinetic modelling.

Five various NO-TPD cycles were performed on the adsorbents prepared in **Paper V**. The cycle started with an adsorption step at 80°C for 2 h, with 200 ppm NO, 8% O₂ and 5% H₂O and Ar, and a total flow rate of 550 ml min⁻¹. Thereafter the NO was shut off and the temperature ramped up to 550°C at a rate of 20 °C/min, with the gas containing 8% O₂, 5% H₂O and Ar. Additional NO-TPD experiments were performed in four other cycles: Cycle 2 was conducted with 300 ppm NO, 8% O₂ and 5% H₂O; Cycle 3 with 300 ppm NO, 8% O₂ and 5% H₂O, where the total flow was changed to 750 ml min⁻¹; Cycle 4 with 400 ppm NO, 8% O₂,

5% H₂O and a total flow of 550 ml min⁻¹ and, finally, Cycle 5, which was the same as the first cycle in order to investigate the stability of the adsorbent. The main focus of this paper was to study the effect of phosphorous on Pd/SSZ-13 in passive NO_x adsorption processes; the results were focused on Cycle 1 in the NO-TPD experiments.

3.3 Characterisation techniques

3.3.1 Inductively coupled plasma sector field mass spectrometry (ICP-SFMS)

The explicit loadings of the materials on the zeolite supports were measured by ICP-SFMS for all freshly-prepared samples: this analysis was performed by ALS Scandinavia AB. The basics of this method involve ionising the sample with inductively coupled plasma and then separating and quantifying these ions using a mass spectrometer (MS).

3.3.2 Specific surface area analysis (BET)

According to the theory suggested by Brunauer, Emmett and Teller in 1938, the total surface area of dry and solid materials, such as supported catalysts, can be measured by nitrogen physisorption⁷⁶. The BET-method is based on various simplifications⁷⁷, which include the following assumptions:

- All available sites have the same energy, but each site can accommodate only one adsorbed molecule of the adsorbent.
- Should multi-layers be formed, adsorbed molecules will not have lateral interactions.
- The rates of adsorption and desorption will be equal, regardless of the layer⁷⁸.

Taking these assumptions into account, specific surface area is therefore measured based on the volume adsorbed by the adsorbate (N₂). This method has been useful for measuring the surface area of macroporous (pore diameter >50 nm) and mesoporous (pore diameter 2-50 nm) materials, but can be deceptive for microporous (pore diameter <2 nm) materials⁷⁷, which also includes zeolites. This is due to the difficulty of adsorbate multi-layers forming within small pore volume materials⁷⁹. According to the literature, BET characterization has nevertheless been used to compare the surface area of zeolites because the results are considered to be proportional to the pore volume⁷⁹. In the present study, a Tristar 3000 (Micromeritics) instrument using liquid N₂ at a specific temperature (-195°C) was employed for the characterisation. Prior to the measurements, all the fresh powder samples were degassed overnight in N₂ at 220°C and under vacuum.

3.3.3 Scanning transmission electron microscopy (STEM)

This technique provides information of the morphology, structure, crystallography and elemental composition of various materials. It is possible to acquire high resolutions images of the particles down to the nanometer scale. The concept of this method is to accelerate a beam of electrons towards a powdered sample. The electrons can either pass through the sample with no interaction or be scattered by the atoms within it. Scattered electrons can gain a certain angle, allowing them to be discovered by a detector placed on the optical axis. These non-uniform electrons that are thus collected can create an image, the resolution of which depends on the thickness of the sample. This imaging technique requires thin samples because thick samples are non-transparent due to multiple backscattered electrons⁸⁰. In this study, TEM was employed to analyse the particle size of the noble metals and their distribution in the various samples. The powders used were scraped from the monoliths after the reactor experiments were completed and distributed on carbon copper TEM grids (**Paper I**); degreened (see Section 3.2) samples were used in **Papers II** and **V**. All samples were analysed with a FEI Titan 80-300 TEM.

3.3.4 Environmental scanning electron microscope (ESEM)

An environmental scanning electron microscope was employed in **Papers III** and **V** to identify the thickness of the washcoat and the position of the phosphorous, respectively. The instrument used was a Quanta 200 ESEM equipped with an energy dispersive X-ray (EDX) system (Oxford Inca).

3.3.5 Energy dispersive X-ray (EDX)

An energy dispersive X-ray (EDX) system was used to gain information of the elemental composition in a specific area. This method basically depends on excitation of electrons from the inner shell after bombarding the sample with an electron beam. An electron from the outer shell then starts to fill the hole in the core and energy is released as an Auger electron or X-ray. The detector measures the X-ray energies emitted which are characteristic of the elements present in the sample⁸⁰. **Papers I** and **II** include EDX mapping images to investigate the distribution and location of both Pd and La particles. This was carried out with a FEI Titan 80-300 microscope (the same instrument as used in the TEM analysis). In **Paper V**, EDX mapping was carried out with a FEI Quanta 200 Environmental SEM (ESEM) coupled with an Oxford X-max 80 EDX detector for the elemental mapping of Pd, P, Si and Al, along with a line scan profile of Al, Pd and P, to confirm the overlap and co-existence of the elements

in the same area. The same method was used in **Paper III** for the elemental mapping of Si and Al in order to measure the thickness of the monolith washcoat.

3.3.6 X-ray photoelectron spectroscopy (XPS)

XPS analysis is an important technique for analysing not only the elemental compositions of a sample's surface but also the chemical nature of the oxidation state of the atomic species. In this method, the sample is placed in an ultra-high vacuum chamber and a monochromic X-ray beam is used to irradiate it with high energy; the kinetic energy detected gives the binding energy of these photoelectrons⁸¹. XPS analysis was used to identify the oxidation state of Pd in **Papers I-III** utilising ultra-high vacuum on a Perkin Elmer PHI 5000C ESCA system equipped with a monochromatic Al K X-ray source with a binding energy of 1486.6 eV. The reference PdO material used in this study was sourced from Sigma-Aldrich (99.97% trace metals basis) and, for reference, C1s with a binding energy of 284.8 eV was used. XPS measurements were conducted in **Paper IV** to investigate the deactivation effect of phosphorous by identifying the oxidation states of P on Pd/SSZ-13.

3.3.7 X-ray powder diffraction (XRD)

The X-ray powder diffraction method is used to study the crystalline structure of samples in a powder form. Various studies can be conducted based on XRD measurements, e.g. it can be used to determine whether or not the synthesized zeolite exhibits the correct crystalline structure, or if a specific reaction condition caused any deformation of the zeolite structure^{30, 82}. The samples are placed between the detector and X-ray source, which are located within an angle of 2θ from each other. The atoms in the sample scatter the incident X-rays and the detector provides the spacing of the atomic planes, using information from the constructively interfering scattered X-rays, by applying Bragg's law ($d = n\lambda / 2\sin\theta$)⁸³. In **Paper II**, powder X-ray diffraction (XRD) was performed on both degreened and reacted samples in a SIEMENS diffractometer D5000, which operates with Cu K α radiation ($\lambda=1.5418 \text{ \AA}$) at 40 kV and 40 mA. The range of $5^\circ - 60^\circ$ (step size of 0.01) was used for data collection to investigate the size of the Pd crystals after reaction with and without lanthanum. The same procedure was used in **Papers III** and **V**, with a measurement range of 5° to 50° and a rate of 0.01 $^\circ$ /min. In both papers, the measurements were initially made to confirm the structure of the synthesized SSZ-13 zeolite; this analysis was also used in **Paper V** to show the sintering behaviour of Pd particles resulting from exposure to CO in multiple cycles. In **Paper IV**, XRD measurements were conducted to confirm the structure of synthesized SSZ-13 and to examine whether the zeolite framework had suffered from

dealumination or structural issues following phosphorous poisoning, using the data collection range 5° to 45° using a step size of 0.01.

3.3.8 Temperature programmed oxidation (TPO) and reduction (TPR)

Important information regarding the interaction of oxygen with materials available in the samples in question can be obtained via oxidation and O₂ desorption. These analyses were performed by placing the powder samples in a vertical quartz tube (inner diameter of 5 mm) inside an electric furnace. Mass flow controllers (MFC) were connected to the system to regulate the flow and mixing of gas and the composition of the outlet gas was measured by a Hiden HPR-20 QUI mass spectrometer. TPO was conducted in **Paper I** to observe the effect of La on the oxidation/dissociation behaviour of the Pd/PdO in the PNA adsorbent. 50 mg of the fresh powder sample was loaded in a quartz tube with a gas flow of 20 ml min⁻¹ and Ar gas as the inert balance. The pretreatment step involved reducing the adsorbent at 600°C for 30 minutes in 1% H₂ and later cooling it to 100°C under the same conditions. The TPO experiment was continued by flushing with Ar at 100°C for 25 min, followed by the addition of 250 ppm O₂ in Ar over the sample for 90 min. Thereafter, the oxygen consumption and subsequent desorption were recorded by increasing the temperature to 800°C at a rate of 20°C/min in the same gas mixture; the final step was isothermal at 800°C for 60 min.

In **Papers II** and **IV**, O₂-TPD was performed on both degreened and reacted samples to observe both the uptake and desorption of oxygen. 50 mg of each powder sample was loaded in the quartz tube before 3 vol.% O₂/Ar at 25°C, with a gas flow rate of 20 ml min⁻¹, was applied for 5 minutes. The same gas mixture was thereafter retained while increasing to 400°C and staying isothermal for 30 min. The experiment was followed by cooling down to room temperature with the same gas composition, and remaining at these conditions for 30 min. After one hour of only Ar flushing at room temperature, the desorption step was started by increasing to 800°C at a rate of 20°C/min in the presence of Ar.

Hydrogen can be used as a reducing agent while heating the pre-oxidized sample in order to identify the temperature of reduction: the detected consumption temperature for hydrogen corresponds to the reduction temperature. In **Paper IV** the evaluated monoliths was crushed and loaded into the quartz tube (50 mg). The powders were treated with 7% O₂/Ar at 500°C for 1 h with the gas flow rate of 20 ml min⁻¹. After reaching room temperature (25°C), 0.2% H₂/Ar was inserted into the quartz tube and the temperature ramped up to 600°C.

3.3.9 Solid state nuclear magnetic resonance (NMR)

The chemical composition, local structure and dynamic properties of a solid can be determined by solid state NMR (ssNMR)⁸⁴. An external magnetic field and radio frequency pulses are used to obtain signals from the surface of various species⁸⁵. In **Paper V**, solid state ²⁷Al NMR spectra allowed the interaction possible between phosphorous and Al in the zeolite to be comprehended. The spectra were gathered for degreened and reacted non-poisoned and P-poisoned samples in a Bruker Avance III 500MHZ spectrometer using a 4 mm double-resonance MAS probe. The rotor was set to spin at 5000 Hz and a single pulse experiment (hpdec) was used with an ¹H decoupling (SPINAL64) of about 83 kHz. The final spectra were normalised using the weight of the samples and the accumulated scans.

3.3.10 In-situ DRIFT spectroscopy

Diffuse reflectance infra-red Fourier transformed (DRIFT) spectroscopy was used to characterise the surface species. This is a common method used to identify various material sites by investigating the adsorption of probe molecules, including CO and NO. The transition between the vibrational energy levels of compounds adsorbed on the surface of a species can produce IR from specific frequencies that can be detected by this technique⁸⁶. In this analysis, the powder sample was placed on a porous grid in a reaction cell equipped with a CaF₂ window. A Vertex 70 spectrometer (Bruker) with a liquid nitrogen cooled MCT detector was used; the flows of inlet gases were controlled by multiple MFCs and the water vapour was controlled by a CEM system.

Paper I used DRIFTS analysis to study the effect of La in creating new sites for the adsorption of NO_x on the adsorbent, and the thermal stability of the NO_x species on those sites, for the sample in question: freshly calcined powder produced from the reference and La-promoted samples were used. The experiment started with 60 min of degreening using 8% O₂, 1000 ppm NO and Ar as the carrier gas at 550°C, followed by a pretreatment step at the same gas temperature and 8% O₂ in Ar for 2 hours. After cooling down to 80°C, a background spectrum was acquired in the same gas mixture. The spectra were collected while introducing 1000 ppm NO to the 8% O₂ in Ar for 30 min.

In **Paper II**, DRIFTS analysis investigated the stability of the promoted sample after multiple NO-TPD experiments in the presence of CO for Pd/BEA. Prior to this analysis, freshly prepared samples were degreened in the flow reactor (see Section 3.2). A pretreatment step was performed for 15 min with 8% O₂, 1% H₂O and Ar as carrier gas at 550°C. Thereafter the chamber was cooled down to 80°C in the same gas mixture and a background spectrum

acquired. The first spectra were collected during the introduction of 200 ppm NO, 1% H₂O and 8% O₂ for 15 min before the other spectra were collected, with 200 ppm NO and 4000 ppm CO with 1% H₂O and 8% O₂ in Ar for 15 min. This was followed by heating the chamber to 550°C for 15 min for a desorption step in the same gas mixture. These adsorption and desorption cycles were repeated and recorded three times, with a new background spectrum being collected prior to each cycle.

In-situ DRIFTS was conducted in **Paper IV** in order to study the sintering mechanism of Pd during the adsorption and desorption of NO for Pd/SSZ-13. The measurements were conducted for both degreened and reacted samples employing the same procedure as in **Paper II**, but without repetition of the NO-TPD for the DRIFTS measurements. The DRIFTS analysis performed in **Paper V** examined the surface species of Pd/SSZ-13 post phosphorous poisoning. The samples were pretreated in the same way as in **Paper II**, continuing with an adsorption step using 200 ppm NO, 1% H₂O and 8% O₂ for 15 min followed by desorption at 550°C with the same gas mixture. 200 ppm NO, 400 ppm CO, 1% H₂O and 8% O₂ were then injected at 80°C for 15 min, prior to a desorption step with the same gas mixture.

Chapter 4

4. Palladium supported on modified beta zeolite

It has been shown that Pd/BEA is an effective material for NO_x adsorption at low temperatures^{22, 26}. The temperature of NO_x desorption from Pd/BEA can however be modified with the aim of achieving a more beneficial temperature window for the downstream SCR system. Therefore, the effect of different promoters on Pd/BEA in PNA processes was studied in **Paper I**; an investigation into the effect of water and H₂ pretreatment was also conducted on the PNAs. Subsequently, the best modified Pd/BEA adsorbent was investigated in **Paper II** for its activation stability after multiple cold start cycles in the presence of high concentrations of CO.

4.1 PNA activity tests

4.1.1 Study of different promoters on Pd/BEA and hydrogen pretreatment effects

Three different promoters, namely ceria, zirconia and lanthanum on Pd/BEA zeolite with a loading of 10 wt.%, were studied in **Paper I**. As a reference sample, 1 wt.% Pd was loaded on a beta zeolite support with a SAR of 38. Fig. 2 shows the quantity and temperature range of NO_x released during the wet TPD experiments (200 ppm NO, 8% O₂ and 5% H₂O in Ar carrier) for Pd/BEA and the promoted samples, respectively. All the samples were pretreated prior to the main NO-TPD experiments. It is evident from Fig. 2 that the reference sample had the largest release of NO_x compared to the promoted samples: the release

temperature is, however, in a lower range than the temperature window suitable for PNA processes (<200°C). Ce and Zr promoted samples also exhibited NO_x releases at temperatures below the urea dosing temperature. It is interesting that the La-promoted sample showed a different NO_x release behaviour compared with the other modified ones (Fig. 2). The presence of La could effectively shift much of the NO_x release to temperatures above 200°C (between 250-480°C). The positive performance of La in PNA processes was also observed by Ji *et al.*, who reported that an addition of La to Pt/Al₂O₃, reduced the desorption of NO_x at low temperatures and shifted the desorption peak to temperatures greater than 250°C²⁴.

Fig. 2 also shows that an additional adsorption peak of NO_x appeared at temperatures from 80 to 125°C for the La-promoted sample. Later in the experiment, the same wet TPD was repeated directly after cooling back to the adsorption temperature (80°C) in order to investigate the activity for adsorption after the first cycle. The results illustrate the same adsorption/desorption profiles as the first cycle for all adsorbents. Fig. 2 clearly demonstrates that, compared with Pd/BEA and other modified samples, 10%La-Pd/BEA significantly increases the release temperature of NO_x to more appropriate desorption temperatures.

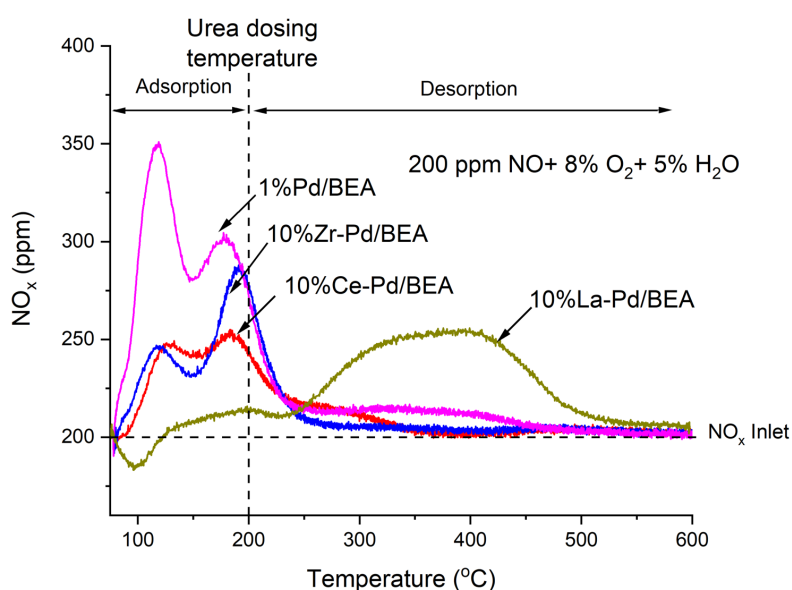


Figure 2. Wet TPD experiment (200 ppm NO, 8% O₂, 5% H₂O and Ar) for the reference (1%Pd/BEA) and promoted samples.

Furthermore, in **Paper I**, the effect of hydrogen pretreatment was investigated for the reference sample (Pd/BEA) and La-modified Pd/BEA. Fig. 3 shows that H₂ pretreatment caused a lower desorption, and thereby also NO_x adsorption, for both samples. The pretreatment step led to a reduction of ca. 40% in desorption for the Pd/BEA sample but only ca. 18%

reduction for the La-promoted sample. It is apparent that the effect of hydrogen pretreatment was significantly smaller on the La-Pd/BEA sample. Also, the hydrogen pretreatment resulted in a small shift in the NO_x desorption temperature to lower values, but it was still above 200°C . It is therefore clear that the presence of H_2 during degreening caused a decrease in the adsorption capacity of NO_x (see Section 2.2.3). The La-promoted sample was less sensitive to hydrogen pretreatment under wet condition. This was studied in greater detail with TPO characterisation, as discussed in Section 4.2.

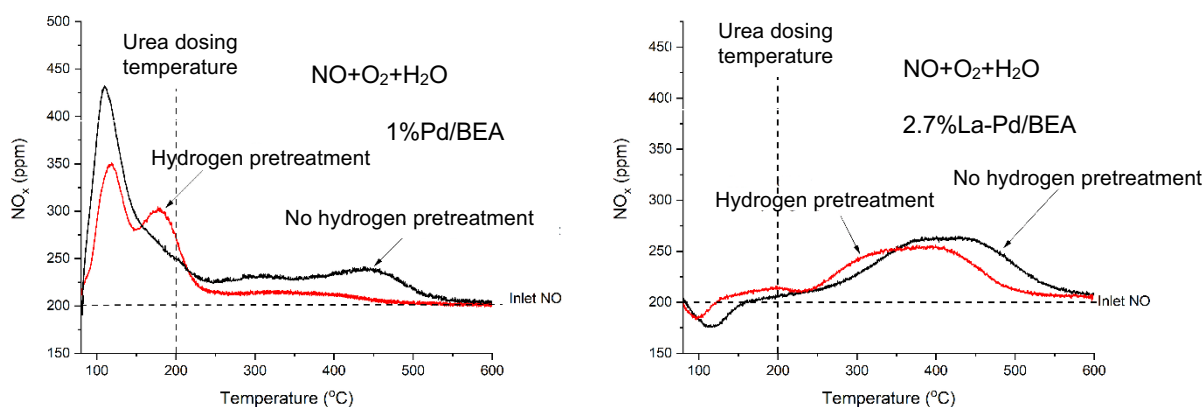


Figure 3. H_2 pretreatment effect in wet TPD (200 ppm NO, 8% O_2 , 5% H_2O and Ar).

4.1.2 Various La loadings and the effect of H_2O

In Paper I, the effect of five different La loadings on Pd/BEA were also studied, using the same NO-TPD and without a hydrogen pretreatment step. Lanthanum, as a promoter, was loaded in the range of 2.7-10 wt.% on Pd/BEA. The results in Fig. 4a show that 2.7 wt.% and 10 wt.% La had lower desorptions of NO_x compared with other La loading values. A possible reason for the lower values of NO_x storage and release for the 10 wt.% La sample could be that blockage of the pores reduces the dispersion of Pd; insufficient loading of lanthanum on the 2.7 wt.% could lead to the formation of stable NO_x species being less likely. Yet, the 2.7%La-Pd/BEA sample had the most suitable temperature release for a PNA process: $200\text{-}400^\circ\text{C}$ ²⁸. Other loadings of La (3.5, 5.4 and 7 wt.%), showed broad releases of NO_x at temperatures higher than 200°C , with a maximum around 350°C . A small desorption peak appeared at lower temperatures for 3.5 and 7 wt.% La-modified samples, which was not detected in the case of 5.4 wt.% La.

At the same time, all samples studied were examined under dry conditions to obtain a better understanding of the H_2O effect in the PNA process (Fig. 4b). As expected, all

samples had a significantly larger NO_x release (and thereby a greater storage capacity) in the absence of water: this is due to the fact that more storage sites are available^{21-22, 25} because there is no blockage by water species. However, the main desorption peaks were located at temperatures lower than 200°C because of the formation of weaker adsorption bonds. Water is nevertheless inevitable in real exhaust aftertreatment conditions, thus taking its presence in the inlet gas into consideration in an experimental setup therefore leads to a more accurate investigation of the activity of the catalyst.

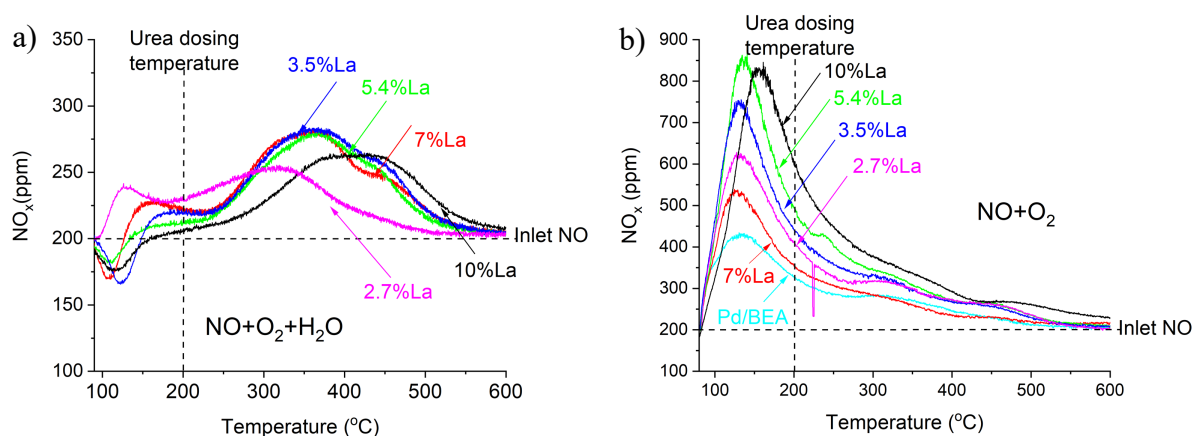


Figure 4. Comparison of different loadings of La. (a) Wet TPD (200 ppm NO, 8% O₂ and 5% H₂O with Ar) without hydrogen pretreatment. (b) Dry TPD (200 ppm NO, 8% O₂ and Ar) for various loadings of La without hydrogen pretreatment.

Regarding the thermal stability of the NO_x adsorbed on La-promoted samples in the flow reactor experiments (**Paper I**), La was suggested as a promising promoter for the Pd/BEA adsorbent. It was also observed that the different concentrations of lanthanum can shift the temperature range of NO_x release. The desorption temperature of NO_x depends on various factors such as the synthesis method, composition of the materials and/or gas, aging conditions and ramping rate^{24, 26, 37, 71}. The optimum temperature range for NO_x release is however between 200°C and 400°C, since desorption at higher temperatures makes it difficult to regenerate the adsorbent during standard operating conditions. After examining the results given in Fig. 4a, 2.7% La-Pd/BEA was chosen as the focus of the study in **Paper II** regarding the effect of lanthanum modification on the stability of the adsorbent during multiple NO-TPDs with high concentrations of CO.

4.1.3 Effect of CO on the sequential passive adsorption of NO_x

For this study, all samples were first degreened (Section 3.2); adsorption was conducted at 80°C and desorption whilst the temperature was being increased to 500°C, with a gas mixture of 200 ppm NO, 4000 ppm CO, 1% H₂O and 8% O₂ in Ar. Figs. 5 and 6 display the profiles of NO_x desorption during 10 sequential TPDs for Pd-La/BEA and Pd/BEA. The conclusion can be drawn that the reference Pd/BEA sample lost much of the amount of NO_x it released during the cycles, suffering a reduction of around 65% by the 5th cycle compared with the first cycle. Moreover, beyond the 5th cycle, degradation continued at a slower pace: 11% loss in NO_x desorption from the 5th to 10th cycle, i.e. 76% in total. This degradation was also reported by Theis *et al.* for Pd/BEA during multiple cycles of measuring NO_x storage using 900 ppm CO and 300 ppm H₂²⁸. It is interesting that the results in Fig. 6 show a different behaviour for the La-promoted sample, which had a degradation of about 64% in the NO_x release from the first cycle to the 5th and had no degradation beyond the 5th cycle. The desorption temperature of this sample is not only in a more favourable range for PNA processes: La also helped the Pd/zeolite to reach a more stable behaviour after the 5th cycle. In total, the Pd/BEA sample lost 76% of its NO_x storage capacity, while the Pd-2.7%La/BEA sample lost 64%. In the modified sample, the corresponding desorption peak at low temperatures disappeared and an adsorption peak around 160°C grew during further cycles.

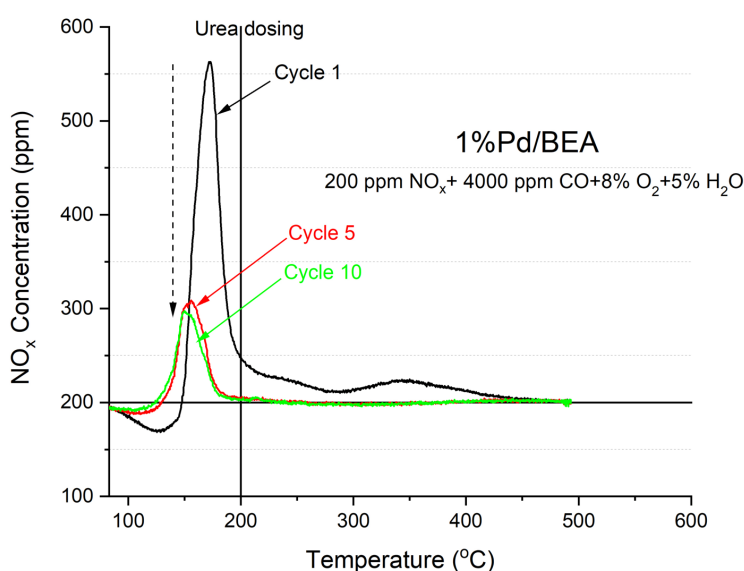


Figure 5. Concentration of NO_x in the repeated TPD experiments, with 200 ppm NO, 8% O₂, 5% H₂O and 4000 ppm CO using the reference Pd/BEA sample.

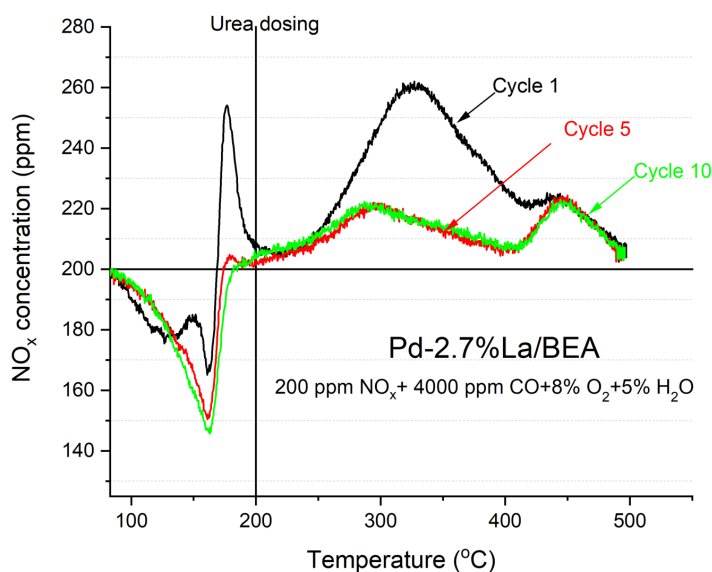


Figure 6. Concentration of NO_x in the repeated TPD experiments, with 200 ppm NO_x , 8% O_2 , 5% H_2O and 4000 ppm CO using the Pd-2.7%La/BEA sample.

In order to understand the role of La in the performance stability of the Pd-La/BEA, a Pd-free sample with 2.7 wt.% La was tested in the same reactor condition (Fig. 7a). The desorption profile illustrated that the desorption process was stable, exhibiting a maximum of around 350°C for this sample. However, this desorption peak is shown as being related to NO_2 only: no NO was detected (Fig. 7b). It can therefore be concluded that La stored some of the NO_x as nitrates and desorbed them in the form of NO_2 at temperatures between 200-400°C. These nitrates can be formed due to a small amount of NO_2 in the feed and/or by conversion of NO on the surface of the sample. On the other hand, Pd-La/BEA desorbed both NO_2 and NO at higher temperatures up until the last cycle, and the total release was still 26% higher than La/BEA (Fig.7c). Thus, it may be concluded that the interaction between La and Pd in Pd-La/BEA can form new adsorption sites that have the ability to release NO at high temperatures, and also that the storage is more stable after multiple cycles. A shift of 20°C towards higher temperatures was observed for the NO_x release peak of the La/BEA samples compared with those of Pd-La/BEA, indicating that the interaction between La and Pd facilitated the desorption of NO_x . A summary of the integrated desorbed NO_x in all the samples is given in Table 4 for two different release temperature ranges, namely P1: <200°C and P2: 200-400°. According to these results, more NO_x was released in both temperature ranges (P1 and P2) for Pd-La/BEA than for La/BEA from Cycle 1 to 10. Thus, both Pd and La sites were associated with the storage of NO_x .

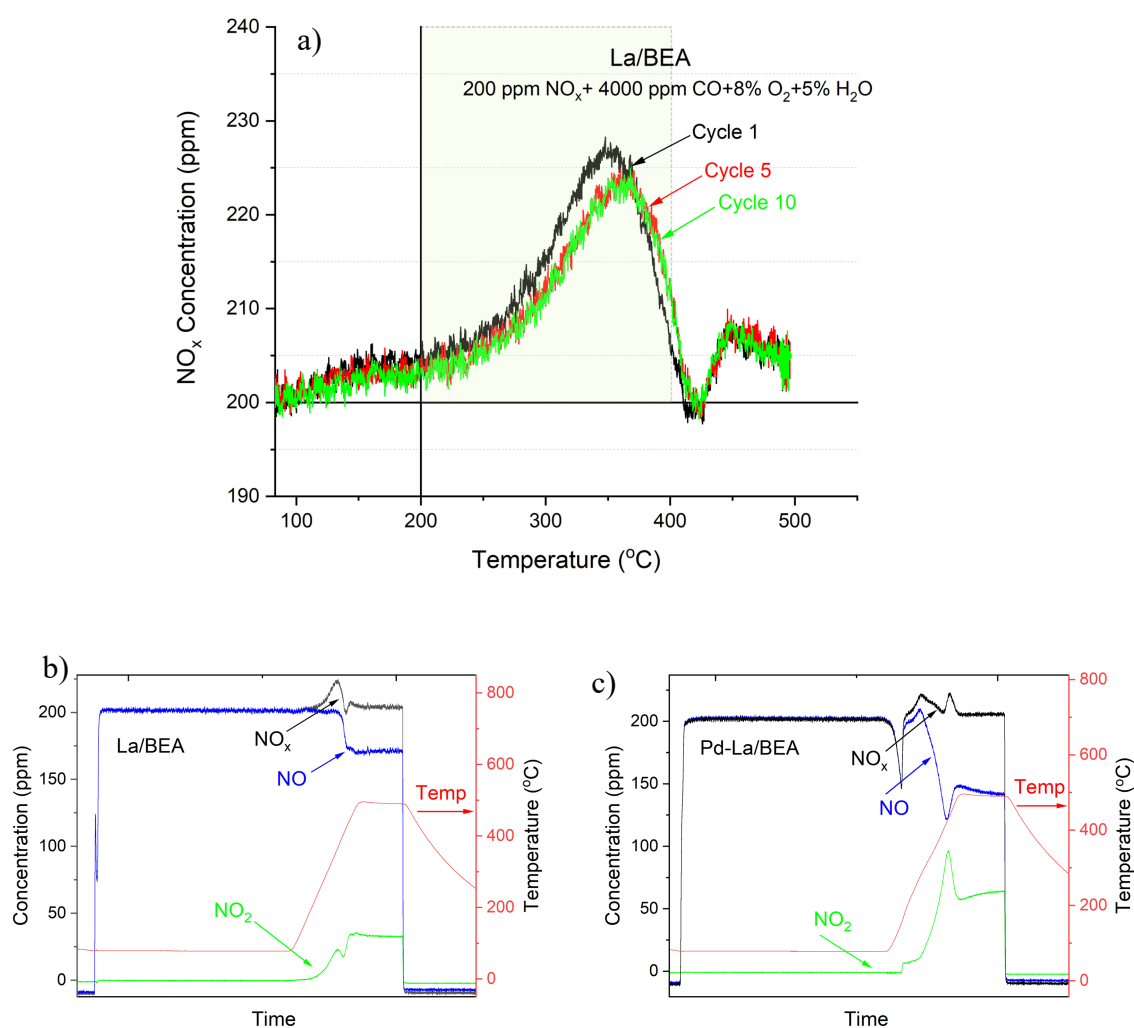


Figure 7. (a) Concentration of NO_x in the repeated TPD experiments using La/BEA. (b) NO_x, NO, NO₂ concentrations for the 10th cycle of La/BEA and c) Pd-La/BEA.

Table 4. Integration of the NO_x desorption peaks of La/BEA, Pd/BEA and Pd-La/BEA.

	Cycles	P1 (<200°C)		P2 (200°C<x<400°C)	
		NO _x (μmol)	Peak Temp	NO _x (μmol)	Peak Temp
La/BEA	1	0.31	-	5.59	351°C
	5	0.34	-	4.87	363°C
	10	0.37	-	4.70	364°C
Pd/BEA	1	13.0	172°C	8.30	345°C
	5	4.6	156°C	0.08	-
	10	4.1	152°C	0.01	-
Pd-La/BEA	1	1.13	177°C	14.3	327°C
	5	0.03	-	5.20	296°C
	10	0.06	-	5.71	289°C

4.2 Physicochemical characterisation

The actual contents of Pd and La on the support were measured by ICP-SFMS (Tables 1 and 2, Section 3.1.2) and the surface area of all the samples were measured using N₂ physisorption (BET). It was apparent that increasing the La concentration reduced the specific surface area: a reduction that was around 30% from 0 to 10 wt. % La. This reduction was seen in the pore volume as well (Table 5), which is due to blockage of the pores and the available surface area with the lanthanum.

Table 5. BET surface areas and pore volumes.

Sample Type	SBET (m ² /g)	Pore Volume (cm ³ /g)
1%Pd/BEA	597.7	0.35
2.7%La-Pd/BEA	555.1	0.32
Pd-2.7%La/BEA	540.0	0.32
3.5%La-Pd/BEA	519.0	0.31
5.4%La-Pd/BEA	477.0	0.29
7%La-Pd/BEA	427.5	0.26
10%La-Pd/BEA	414.5	0.25

TEM analysis in Fig. 8 shows the morphology of the Pd particles in the reference Pd/BEA sample and the 5.4%La-Pd/BEA sample (taking an average loading of La for the range studied). The samples used for this analysis in **Paper I** were acquired after the activity test and were scraped off from the monolith. It should be noted that ion-exchanged Pd²⁺ species cannot be detected by STEM, since it is only possible to see an overview of the particles dispersed on the surface with this technique. The images indicated a reasonably good distribution of Pd particles in the reference sample. Fig. 8a shows that the average size of the Pd particles was around 2 to 5 nm, while Fig. 8b displays agglomerated particles ranging from 20 to 50 nm for the 5.4%La-Pd/BEA sample. This agglomeration could explain the lower NO_x adsorption/desorption (~ 25%) ability of the La-promoted sample (Fig. 2). It is an effect that can be related to the fact that fewer available ion-exchange positions remain, which can lead to a poorer dispersion of Pd species²¹. Other studies have found that the presence of La causes occupancy of Al₂O₃ defect sites or prevents the formation of highly dispersed oxygen-rich palladium species^{24, 87}.

In **Paper II**, the materials analysed were degreened (at 750°C for one hour with 500 ppm NO, 8% O₂, 5% H₂O and Ar) samples of 2.7%La-Pd/BEA and Pd-2.7%La-BEA used to examine the particle distribution. Fig. 9a shows that the sizes of the agglomerated particles

in the 2.7%La-Pd/BEA were between 30 and 50 nm. An improved distribution of metals was observed for the Pd-2.7%La-BEA sample, on the other hand, which had an average particle size of 10-20 nm (Fig. 9b). These results show that the sequence of component loading can also affect the particle distribution. More ion-exchange positions were available in Pd-2.7%La/BEA, and a better distribution of Pd was thus achieved. Therefore, this sample was used for the NO-TPD study and characterizations in **Paper II**.

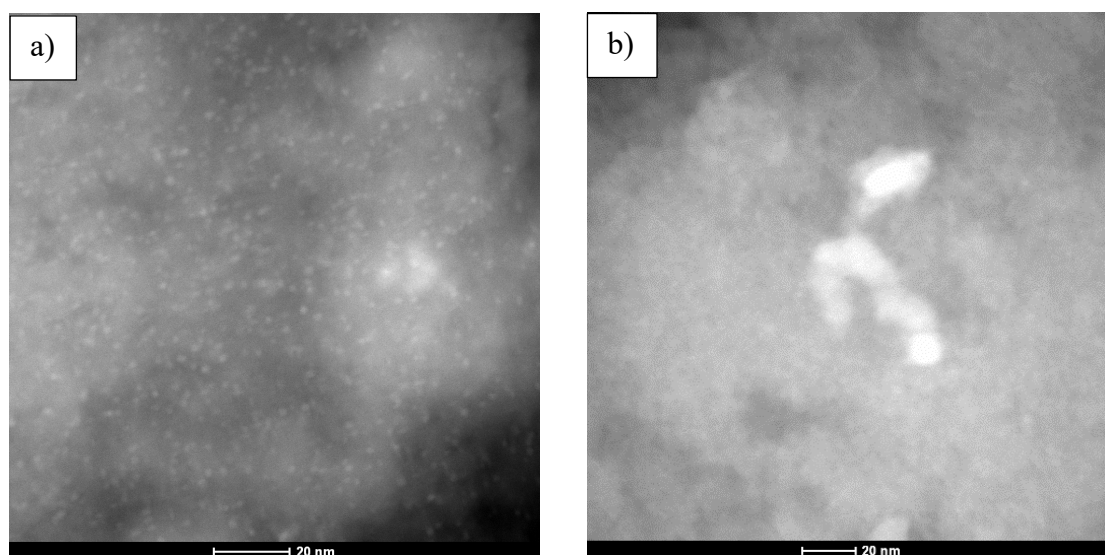


Figure 8. (a) STEM images of 1%Pd/BEA at 20 nm. (b) STEM images of 5.4%La-Pd/BEA sample at 20 nm magnifications.

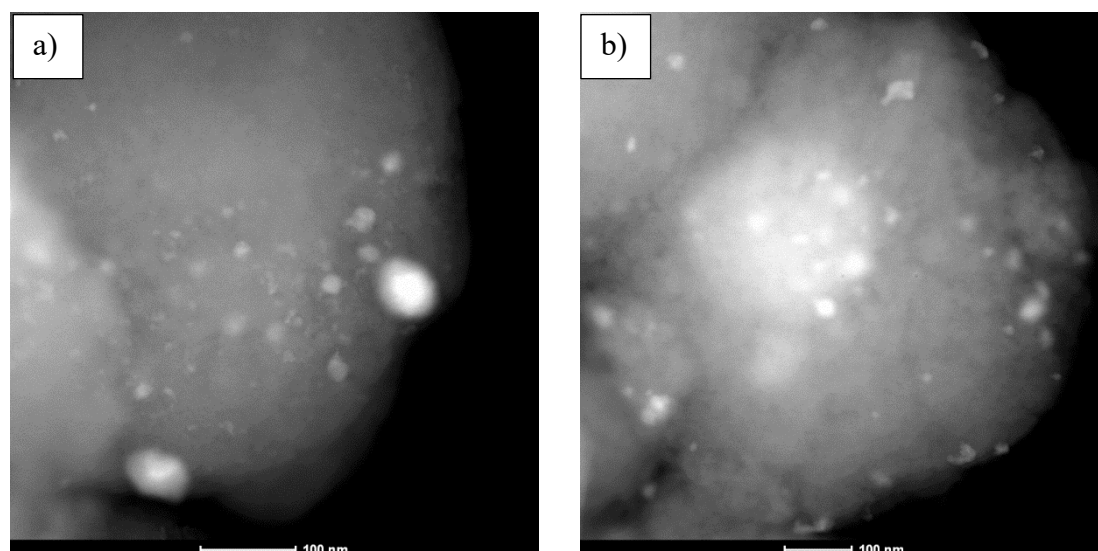


Figure 9. (a) STEM images of 2.7%La-Pd/BEA at 100 nm. (b) STEM images of Pd-2.7%La/BEA sample at 100 nm magnifications.

TPO analysis was performed on freshly prepared powder samples in **Paper I**. After the hydrogen pretreatment step, the sample was exposed to 300 ppm O₂ in Ar at 100°C for 90 min in order to reach a saturated state. The temperature was then increased to 800°C at a

rate of 20°C/min, with the same inlet gas mixture, in order to observe the oxygen desorption peaks. Based on the results in Fig. 10a, it can be concluded that, even with moderate amounts of La, the consumption peaks shifted to lower temperatures, which indicates that the uptake of oxygen was elevated in the modified samples. Furthermore, increasing the loading of La in the tested samples gradually enhanced the stability of oxygen adsorbed. Hoost *et al.* claimed that the presence of La with Pd/Al₂O₃ created a new oxidation mode for Pd, which was assumed to result from Pd-La₂O₃ interactions⁸⁷. The oxidation behaviour of La was investigated by studying a sample of 2.7%La/BEA using the same TPO experiment (Fig. 10b). Lanthanum is known to be a very stable material⁸⁸, and the profile therefore exhibited neither the uptake nor the release of O₂ with the La/BEA sample. It was established that, in the Pd-2.7%La/BEA sample, the oxidation/reduction characteristics were related to the Pd metal and interactions between Pd and La. It is thereby apparent that Pd is in a more thermally-stable oxidized state after modification with La, which can be one of the reasons behind the increased stability of NO_x observed in the PNA experiments (Figs. 2 and 3).

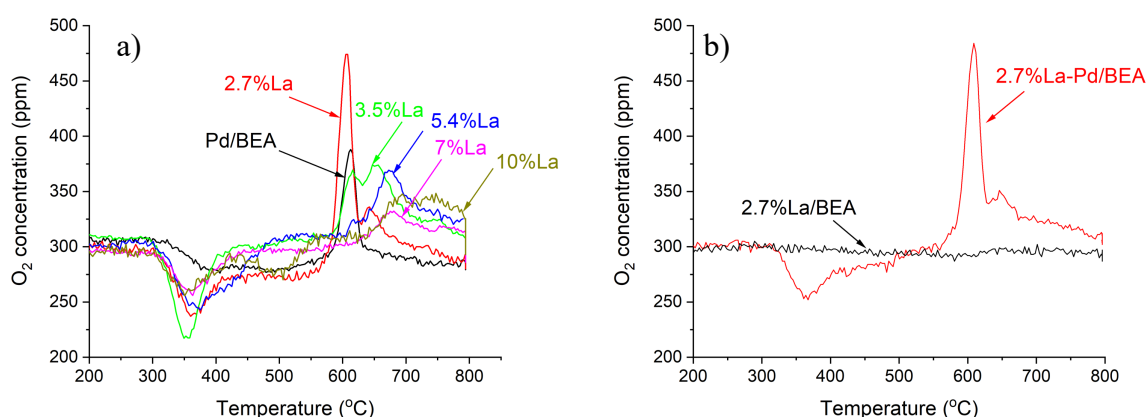


Figure 10. (a) TPO experiment for the reference and La-Pd/BEA samples. (b) TPO experiment for 2.7%La-Pd/BEA and 2.7%La/BEA.

In **Paper II**, O₂-TPD was used to study the properties of Pd/BEA and Pd-2.7%La/BEA in the adsorption and desorption of oxygen to understand the behaviour of the La-modified sample after multiple cycles. Fig. 11 shows the desorption peaks for the degreened materials, as well as the samples used in multiple NO_x TPD cycles (in the presence of high concentrations of CO). Compared to the Pd/BEA sample, the degreened La-promoted sample had an additional peak that appeared between 300-475°C, which can be related to the release of oxygen species adsorbed on PdO_x⁸⁹⁻⁹⁰. As this peak was not detected in the reference Pd/BEA sample, it is suggested the presence of La: it could be related to the fact that more large Pd particles were formed on the La-Pd/BEA sample than on the Pd/BEA sample, as observed in

the TEM analysis (Figs. 8 and 9). The results in Fig. 10b show no adsorption and desorption of oxygen for the La/BEA sample, so the peak detected at 434°C in Fig. 11b can be related to oxygen produced from the oxidation of Pd particles in connection with lanthanum. This peak almost disappeared in the reacted sample due to the reduction of Pd species in the presence of CO.

The second desorption peak (between 500-650°C) in the O₂-TPD can be assigned to the release of O₂ from the decomposition of PdO_x clusters while ramping up to higher temperatures⁹⁰⁻⁹¹. Meanwhile, the integrated peak areas of the reacted Pd-2.7%La/BEA and Pd/BEA were 1.1 and 1.7 times higher, respectively, than the fresh ones. This can be due to the formation of more palladium clusters that have a stronger affinity for oxygen adsorption. A comparison of these results indicates that more PdO_x clusters formed during the repeated cycling of the reference Pd/BEA sample, and that the modified sample was more stable towards the formation of PdO_x clusters. According to the literature, the trapping of NO_x at low temperatures in Pd/zeolite adsorbents is the result of the direct coordination of NO onto ionic Pd²⁺ species²². In many studies it has been suggested that the presence of CO can reduce Pd²⁺ species to Pd particles, which can then form agglomerated clusters^{27-28, 92-93}. Thus, the presence of more Pd clusters on the surface will decrease the amount of Pd²⁺ in the Pd/BEA sample and the ability for taking up NO_x will gradually reduce over the cycles, which was also found in the PNA cycles in **Paper II** (Fig. 5). Moreover, the O₂-TPD results suggested that the Pd-La/BEA sample exhibited fewer palladium clusters during cycling with high concentrations of CO, which could explain why the Pd-La/BEA was more stable during cycling.

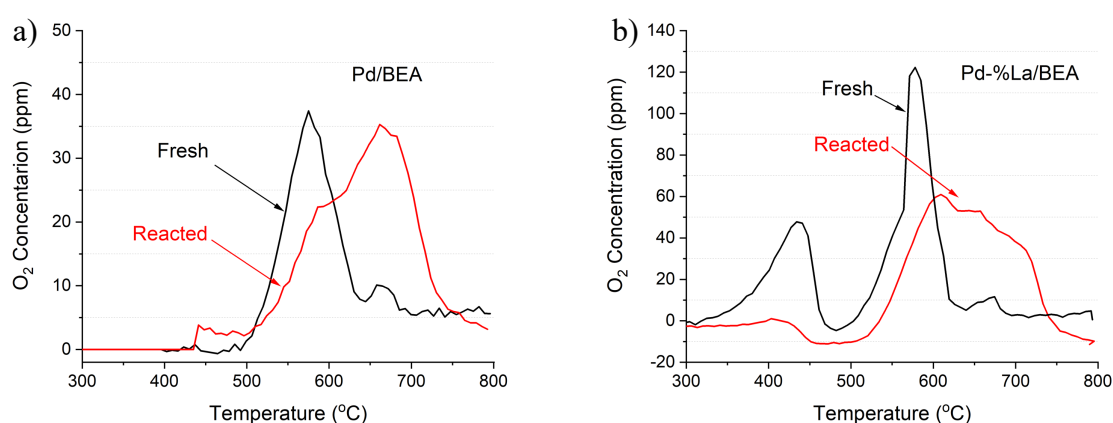


Figure 11. O₂-TPD profiles of the samples of (a) Pd/BEA and (b) Pd-2.7%/BEA.

The XPS analysis performed in **Paper II** confirmed that the reduction of ionic Pd species was due to the presence of high levels of CO. Fig. 12 shows the XP Pd 3d spectra for the degreened and reacted Pd/BEA and Pd-La/BEA samples, respectively. A commercial PdO sample, with two Pd²⁺ peaks located at 336.9 eV(3d_{5/2}) and 342.4 eV(3d_{3/2})²¹, was used as a reference and is shown in the lower panel. Fig. 12a shows a clear shift of the Pd profile towards lower binding energies after multiple NO-TPD cycling with CO. This can be explained by the reduction behaviour of Pd after exposure to CO, which leads to the formation of more clusters as was shown in O₂-TPD. In the case of the reacted La-modified sample, however, the shift is towards higher binding energies that might be due to the migration of Pd atoms from the pores of the zeolite to the surface and the oxygen treatments between the steps can oxidize the Pd clusters. The relative concentration of palladium on the surface of the Pd/BEA sample showed a decrease of 16% after reaction: this value was about 6% for Pd-La/BEA. These results suggest that more Pd clusters are formed on the Pd/BEA sample, causing less available area to be detected on it by XPS. This is consistent with the TPO data as well as the PNA results, where the Pd/BEA sample continued to decrease in efficiency during the 10 cycles.

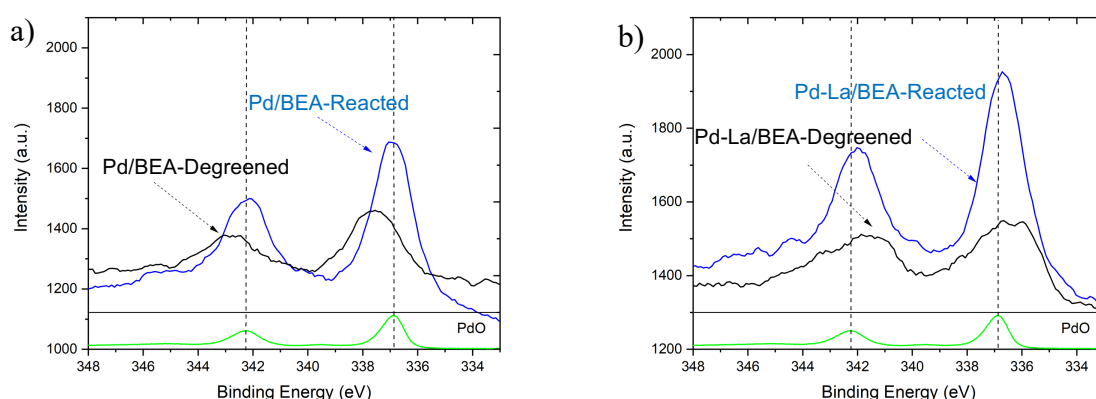


Figure 12. Pd 3d XPS spectra of the degreened and reacted (a) Pd/BEA and (b) Pd-La/BEA samples, using PdO as a reference.

4.3 DRIFT spectroscopy

The DRIFTS analysis in **Paper I** provided important information regarding the nature and quantity of the NO_x species adsorbed on the surface of the adsorbent. The spectra were collected when the freshly prepared samples were exposed to NO and O₂ at 80°C (Section 3.3.6). It should be noted that some NO₂ is formed in the lines prior to the reactor chamber. Fig. 13a shows the spectra collected from the Pd/BEA sample where the highest peaks, which

appeared around 1633 and 1651 cm^{-1} , are related to NO_2 interacting with OH groups²⁴. The next strong peak around 2142 cm^{-1} can be related to NO^+ on Brønsted acid sites²¹⁻²². The peaks at 1830 and 1876 cm^{-1} are assigned to the N = O symmetric stretch of Pd^{2+} -NO nitrosyl species and symmetric stretching vibrations of $(\text{NO})_2$ dimers on Pd, respectively^{21, 26, 94}. Chelating nitrates appeared at 1589 cm^{-1} in this spectrum^{24, 95}. Fig. 13b illustrates the spectra collected from the 5.4wt%La-Pd/BEA sample where the dominant peak was at 1570 cm^{-1} which, according to Ji *et al.*, could be assigned to chelating bidentate nitrates²⁴. A small side peak at around 1480 cm^{-1} was assigned to monodentate nitrates⁹⁶, and the peak that appeared at 1277 cm^{-1} was assigned to bridged nitrates⁹⁷⁻⁹⁸. Moreover, smaller peaks at 1734 and 1876 cm^{-1} were reported as NO dimers on Pd²¹ and Pd^{2+} -NO nitrosyls, respectively. According to the literature, nitrates are more stable than nitrite species and decompose at higher temperatures^{17, 24, 26}. The comparison of the two spectra (Fig. 13) indicated that the presence of La on Pd/BEA enhanced the quantity of nitrate species due to the appearance of a nitrate peak around 1277 cm^{-1} and stronger peaks at 1570 and 1480 cm^{-1} . This was also found by Ji *et al.* with La-Pt/ Al_2O_3 ²⁴. Thus, the DRIFTS results also supported the observations from the NO_x TPD that more thermally-stable NO bonds formed on the 5.4wt.%La-Pd/BEA sample, which can lead to NO_x having a higher desorption temperature (Fig. 6).

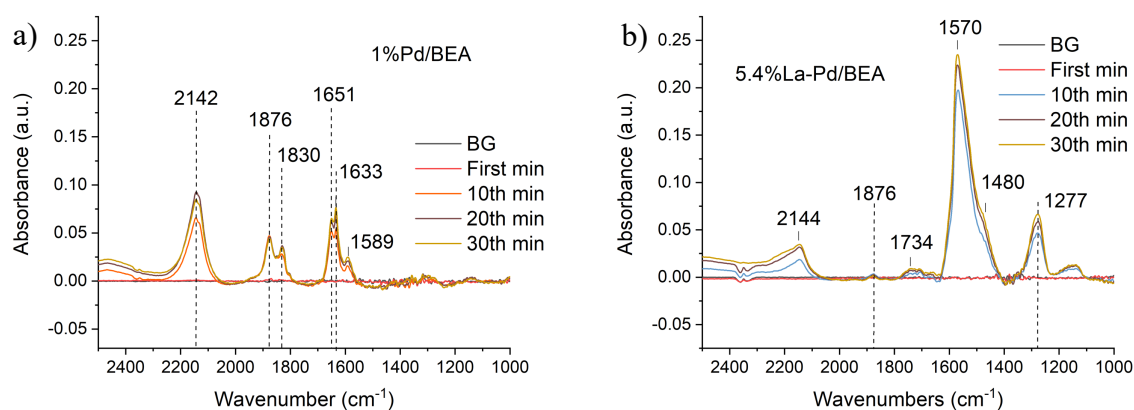


Figure 13. DRIFT spectra obtained during exposure to 1000 ppm NO and 8% O_2 at 80°C for the samples of (a) Pd/BEA and (b) 5.4%La-Pd/BEA.

Paper II included DRIFTS analysis for degreened (Section 3.2) fresh samples, with three cycles of NO-TPD being performed in the presence of H_2O (Section 3.3.6). Fig. 14 compares the NO adsorption step of the 3 cycles for both samples. In each cycle, after exposure to NO for 15 min, CO was also added to the inlet gas. A significant peak appeared around 1813 cm^{-1} for the Pd/BEA sample (Fig. 14a): this is assigned to a linear nitrosyl species, where NO is attached to the cationic Pd^{2+} (Pd^{2+} -NO) located at the exchanged sites^{21, 35}. Peaks around 1633

cm^{-1} and 1653 cm^{-1} were seen in Fig. 13a as well. The strong peak at 1360 cm^{-1} can arise due to the interaction of H_2O with HNO_2 ⁹⁹. Two negative peaks around 2112 cm^{-1} and 2130 cm^{-1} are assigned as linear CO on ionic Pd and $\text{Pd}^+(\text{CO})(\text{OH})$, respectively^{26, 71, 100-101}. The presence of CO in each cycle can cause the formation of its linear bond with Pd^0 and the formation of $\text{Pd}^+(\text{CO})(\text{OH})$ ¹⁰⁰⁻¹⁰¹. These negative peaks after the first cycle appeared while NO removed some of the linear CO on both the Pd^+ and ionic Pd¹⁰². Negative peaks around $3745-3784 \text{ cm}^{-1}$ are caused by the consumption of hydroxyl groups on the zeolite structure, which can occur during the uptake of NO¹⁰³⁻¹⁰⁵. Examining the results in Fig. 14b, the strongest peak of the Pd-2.7%La/BEA sample appeared at 1543 cm^{-1} and is caused by bidentate nitrates⁹⁷⁻⁹⁸. As with the DRIFT spectra in **Paper I**, the peaks of the La-modified sample indicate the presence of larger quantities of nitrates. Moreover, a comparison between Figs. 14a and b indicates that the quantity of the species adsorbed gradually decreased in the Pd/BEA sample for each cycle number, whilst this degradation was small in the La-modified sample, and the performance more stable.

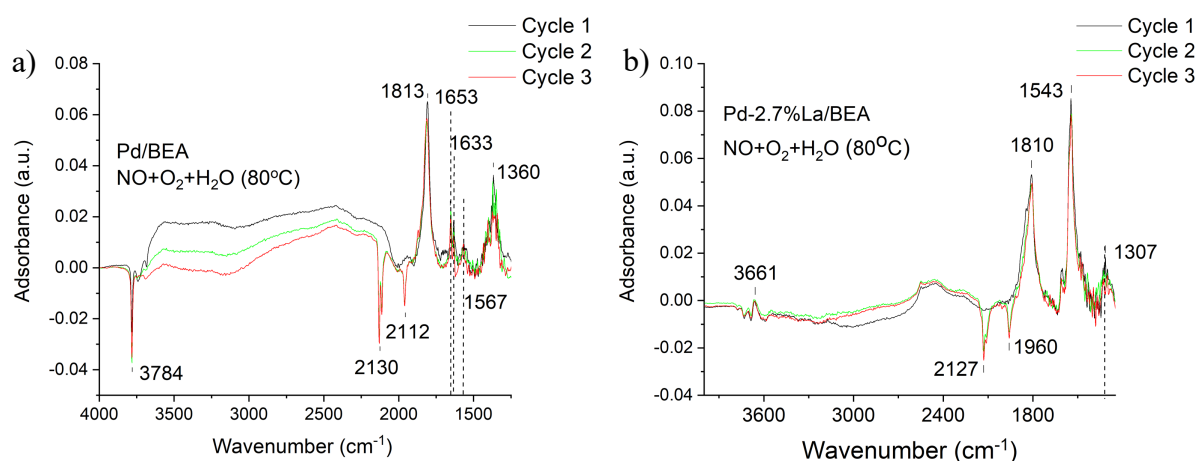


Figure 14. DRIFT spectra obtained during exposure to 200 ppm NO, 8% O₂ and 1% H₂O at 80°C for the samples of (a) Pd/BEA (b) Pd-2.7%La/BEA.

Chapter 5

5. Assisting and degrading behaviour of CO in PNAs

Carbon monoxide is one of the exhaust species inevitable in diesel engines and its effect in PNA processes has been investigated in many studies. Several of these reported low concentrations of CO to be beneficial for the adsorption and desorption of NO_x even after multiple TPD cycles^{25-26,44,55-56}. On the other hand, some studies showed that high concentrations of CO had a degrading effect on the efficiency of PNAs during multiple cycles^{27-28, 57}. Thus, it can be of great interest to understand the mechanism behind the assistance and degradation processes coupled to CO. **Paper III** focused on the effect and mechanism of various low concentrations CO on Pd/SSZ-13 as an adsorbent for PNA and, in **Paper IV**, the study was extended to include higher concentrations of CO. Kinetic models for the mechanisms introduced were developed in both papers.

5.1 Characterisation of the synthesised Pd/SSZ-13

The same synthesised Pd/SSZ-13 (Section 3.1.2), with the same properties, was used in both **Papers III** and **IV** (Table 6). The XRD profile of the synthesised SSZ-13 showed the reference zeolite structure clearly. The thickness of the washcoat on the monolith samples were measured by SEM-EDX mapping and reported to be 70±40 µm (Fig. 15).

Table 6. Elemental analysis, BET surface area and pore volume of Pd/SSZ-13.

Sample	Pd (wt.%)	Si/Al	S_{BET} (m^2g^{-1})	V_{pore} (cm^3g^{-1})
Pd/SSZ	0.98	12	659	0.3

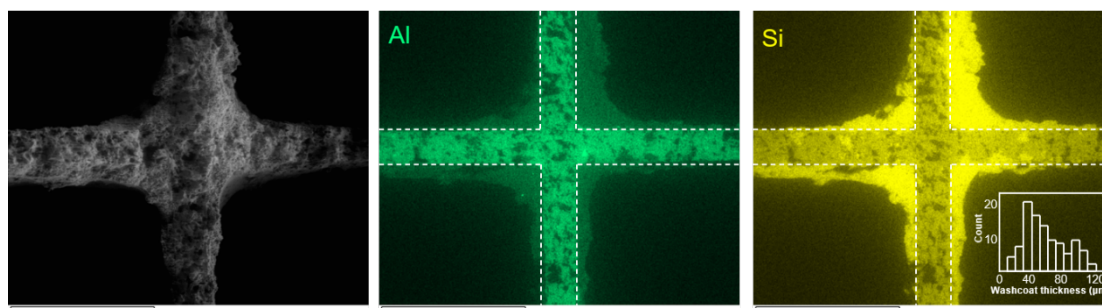


Figure 15. SEM-EDX mapping of Pd/SSZ-13 washcoat for Si and Al. The dashed lines show the cordierite substrate.

5.2 PNA activity tests

5.2.1 Effect of CO on the passive adsorption of NO_x

The flow reactor study conducted in **Paper III** used two different test groups: one with CO and one without (Section 3.2). Initially, Pd/SSZ-13 was evaluated in different NO-TPD cycles with 200-400 ppm NO, 8% O_2 , 5% H_2O and Ar for 7 cycles. The NO_2 concentration in the inlet gas was always below 5 ppm; a degreening step was applied at 750°C for 1h prior to the evaluation cycles. The results of Cycles 1, 2 and 7 (in which the same condition was applied) showed that the adsorbent did not experience any deactivation due to differing NO concentrations and multiple NO-TPDs. Fig. 16 shows the NO, NO_2 and NO_x profiles for Cycles 2, 4 and 6 with 200 ppm, 300 ppm and 400 ppm NO, respectively. The NO profile shows one consumption peak at 166°C and two desorption peaks at 252°C and 371°C . Meanwhile, the NO_2 profile exhibits a desorption peak at 166°C and another at 550°C . NO can oxidize with oxygen and form NO_2 at high temperatures, so the desorption of NO_2 at high temperatures was related to the oxidation of NO. As mentioned previously, desorption of NO_x below 200°C is not efficient for urea dosing in the SCR systems: the two desorption peaks detected at temperatures above 200°C are, however, both efficient for the downstream SCR unit. These three peaks of NO_x release allow the conclusion to be reached that there are different adsorption sites on Pd in Pd/SSZ-13. According to the NO_x/Pd ratio in Table 7, it can be established that the Pd sites were saturated by the low concentration of NO (200 ppm) and, therefore, the ratios storage for

higher concentrations were similar to 200 ppm. Furthermore, the presence of H₂O, along with the formation of PdO clusters on the surface, led to a NO_x/Pd ratio lower than 1.

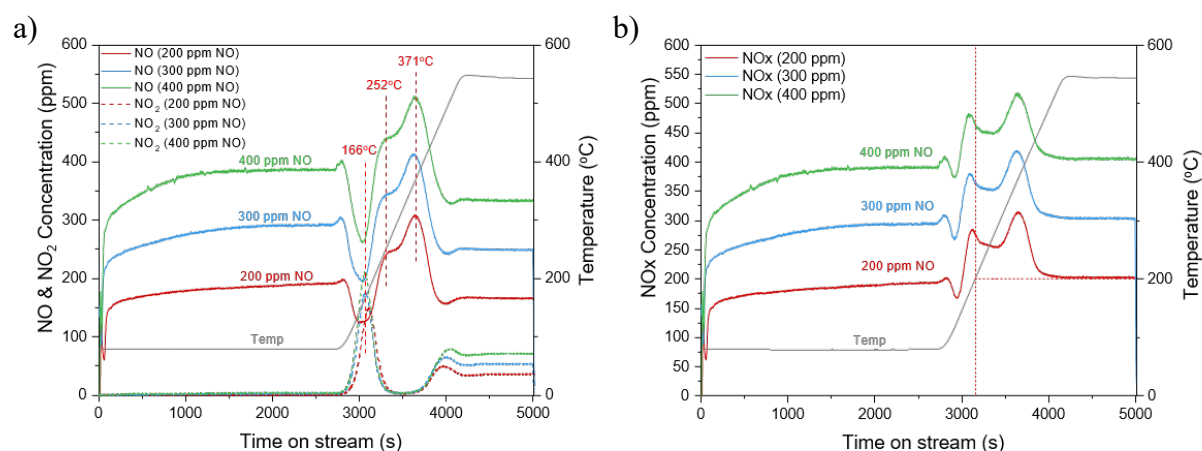
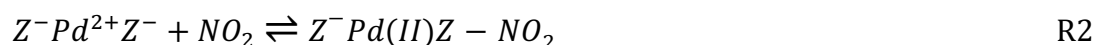


Figure 16. Profiles of the adsorption and desorption steps, with 200, 300 and 400 ppm NO, for (a) NO, NO₂ and (b) NO_x

Table 7. NO_x/Pd ratio of Pd/SSZ-13 with 200, 300 and 400 ppm NO.

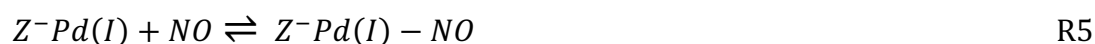
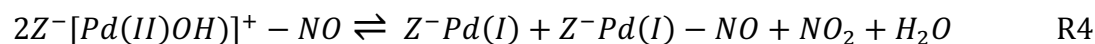
NO _x in feed (ppm)	NO _x /Pd
200	0.64
300	0.67
400	0.64

The mechanism proposed for Pd/SSZ-13 was based on the adsorption and desorption profiles shown in Fig. 16. As mentioned before, Pd²⁺ cations are the main adsorption sites available to NO_x on Pd/zeolite adsorbents^{24-25, 35}; it was therefore suggested that Pd²⁺ can bind with either two Al sites ($Z^-Pd^{2+}Z^-$) or just one, and the charge balanced by an OH group ($Z^-[Pd(II)OH]^+$)^{44, 47, 57, 106}. Accordingly, the following reactions were proposed related to these two sites:



According to the literature, the low binding energy of NO on $Z^-[Pd(II)OH]^+$ when forming $Z^-[Pd(II)OH]^+ - NO$ ^{57, 104} results in this site being easily reduced by NO, and $Z^-Pd(I)$ (R4) is formed when the temperature is increased. This new site has the strongest bond with NO (R5) compared with other Pd²⁺ or Pd⁺ sites^{57, 104, 106}. Therefore,

the two NO desorption peaks at 252°C and 371°C are assigned to releases of NO from $Z^-Pd^{2+}Z^-$ and $Z^-Pd(I)$, respectively. The reduction of $Z^-[Pd(II)OH]^+$ (R4) could explain the NO_2 produced and NO consumed at 166°C (Fig. 16). In order to regenerate the sites, since no deactivation was observed, the $Z^-Pd(I)$ was re-oxidized back to $Z^-[Pd(II)OH]^+$ according to Reaction 6 in the pretreatment step between the cycles.



The formation of PdO clusters on the surface of the zeolite is inevitable when using the impregnation method^{25, 50}. These sites can adsorb NO to form $Pd(NO_3)_2$ and later decompose to release NO_2 at 166°C (R7 and R8). However, the storage capacity of this site is smaller than the other two. The NO_2 produced at higher temperature, which is related to NO oxidation, is described by R9.



A second NO-TPD test was designed in **Paper III** to investigate the effect of low concentrations of CO, and involved 200-400 ppm CO, 200 ppm NO, 8% O_2 , 5% H_2O and Ar for 5 cycles (Section 3.2). Comparing the activity of Cycles 1 and 2 with Cycle 7 (in which the same condition was applied) shows no obvious deactivation during multiple cycles at different CO concentrations (200-400 ppm). Fig. 17 illustrates the adsorption and desorption profiles of NO, NO_2 and NO_x for Cycles 2 and 4 with CO (200 and 400 ppm) and Cycle 1 from the previous test without CO. The desorption peak at low temperature (166°C) that was related to NO_2 was drastically decreased, possibly due to the reduced Pd sites caused by $CO^{25, 107}$: the related reduced sites in this case were $Z^- [Pd(II)OH]^+$ and PdO. The middle desorption peak at 252°C was increased by increasing the CO concentration; the high temperature release (371°C) increased with 200 ppm CO and later decreased with 400 ppm. After exposure to CO, all desorption peaks were above 200°C, which is beneficial for the PNA processes. According to

the NO_x/Pd ratio calculated in the current TPD condition, however, CO did not promote the amount of NO_x adsorbed over Pd/SSZ-13 (Table 8).

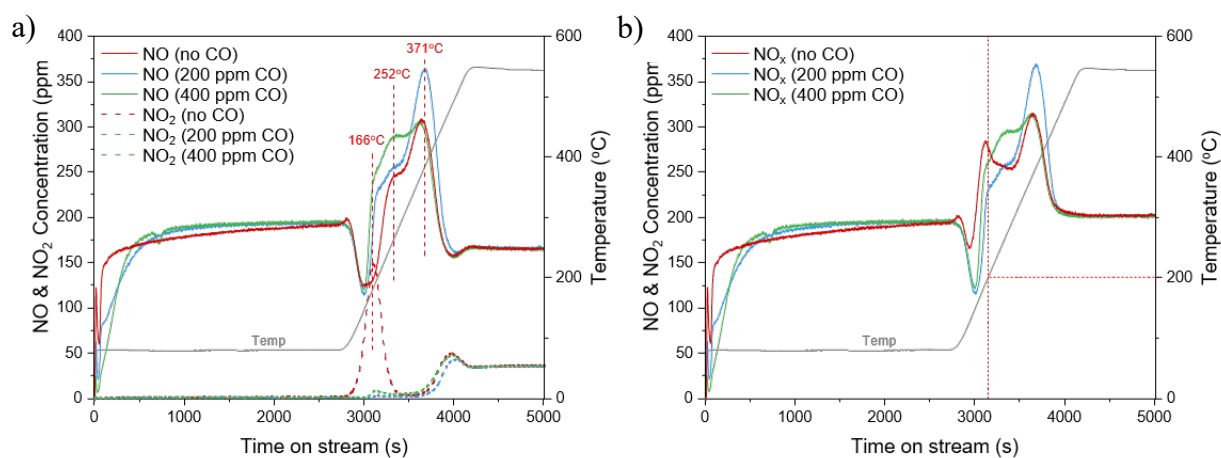
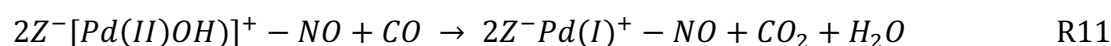
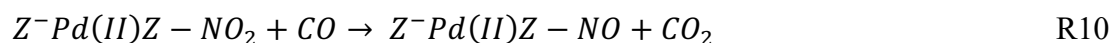


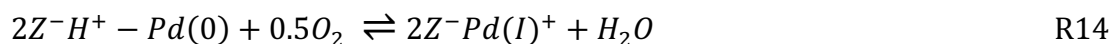
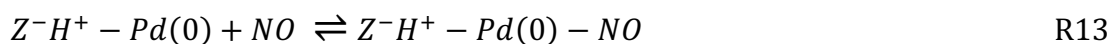
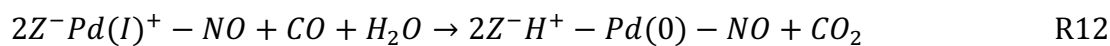
Figure 17. Profiles of the adsorption and desorption steps, with 0, 200 and 400 ppm CO, for (a) NO, NO_2 and (b) NO_x

Table 8. NO_x/Pd ratio of Pd/SSZ-13 with 0, 200 and 400 ppm CO.

CO in feed (ppm)	NO_x/Pd
0	0.64
200	0.69
400	0.68

It was suggested that the main mechanism of the CO-assisted passive adsorption of NO_x is the reduction of the Pd sites, which was also observing by XPS analysis (Section 5.3). In the mechanism proposed, the $Z^-Pd(II)Z^- - \text{NO}_2$ that was formed in R2 was reduced by CO and $Z^-Pd(II)Z^- - \text{NO}$ was formed (R10). Furthermore, the reduction of PdO sites into Pd^0 caused stronger bonds to be formed between the NO and metallic Pd, which desorbed at 371°C (R15 and R17). Lastly, the reduction of $Z^-[\text{Pd}(II)\text{OH}]^+$ sites formed $Z^-Pd(I)^+$ (R11)⁴⁴: these were reduced further to $Z^-H^+ - \text{Pd}(0)$ (R12), resulting in the release of NO at 250°C (R13). Different concentrations of CO influenced the distribution of $Z^-Pd(I)^+$ and $Z^-H^+ - \text{Pd}(0)$, which led to variations in the release of NO_x at temperatures around 250 and 370°C. Reactions 14 and 16 are important for the re-oxidation of reduced active sites in the pretreatment step, since the catalyst was stable in multiple cycles at low concentrations of CO.





5.2.2 Degrading effect of CO on the passive adsorption of NO_x

In **Paper IV** the degrading effect of high concentrations of CO on Pd/SSZ-13 was studied. As in **Paper II**, multiple NO-TPDs were conducted, using 4000 ppm CO, 200 ppm NO, 8% O₂, 5% H₂O and Ar (Section 3.2), to investigate the activity of the Pd/SSZ-13. Fig. 18 illustrates the NO, NO₂ and NO_x profiles of the first two cycles without CO and Cycles 3-15 with 4000 ppm CO. After exposure to CO, the activity decreased drastically from Cycles 3-7 and, from Cycles 7-15, this deactivation was at a slower rate. The NO desorption peaks around 252°C and 371°C disappeared gradually and a new desorption peak arose at 218°C. This new peak shifted to lower temperatures during TPDs, indicating the formation of a new site and the possibility that this had experienced changes during the cycles. The NO₂ desorption peak also underwent deactivation and shifted to lower temperatures. Based on the characterisation experiments in **Paper II**, it was concluded that high concentrations of CO caused not only the reduction of Pd sites but also Pd agglomerations, which led to the deactivation of Pd/BEA. In this paper, it was proposed that such agglomeration occurred in two sintering modes: Ostwald ripening and particle migration. The Ostwald ripening mechanism has been suggested in many studies for describing the effect of high concentrations of CO on the sintering of different metals (Ni, Pd, Rh)¹⁰⁸⁻¹¹¹. In **Paper IV** it was concluded that, during CO exposure, Pd(CO)_x species were formed and then diffused on the zeolite support; when the temperature was increased, they agglomerated and formed larger particles whilst releasing CO. Thereafter, a particle migration mechanism occurred on the agglomerated Pd species resulting from Ostwald ripening, and formed even larger nanoparticles. The rate of sintering via Ostwald ripening is much faster than particle migration¹⁰⁸, so Ostwald ripening occurs during the initial cycles. The rate then decreases because the clusters thus formed are more stable towards this sintering mode¹¹²⁻¹¹³ and particle migration therefore dominates in the later cycles.

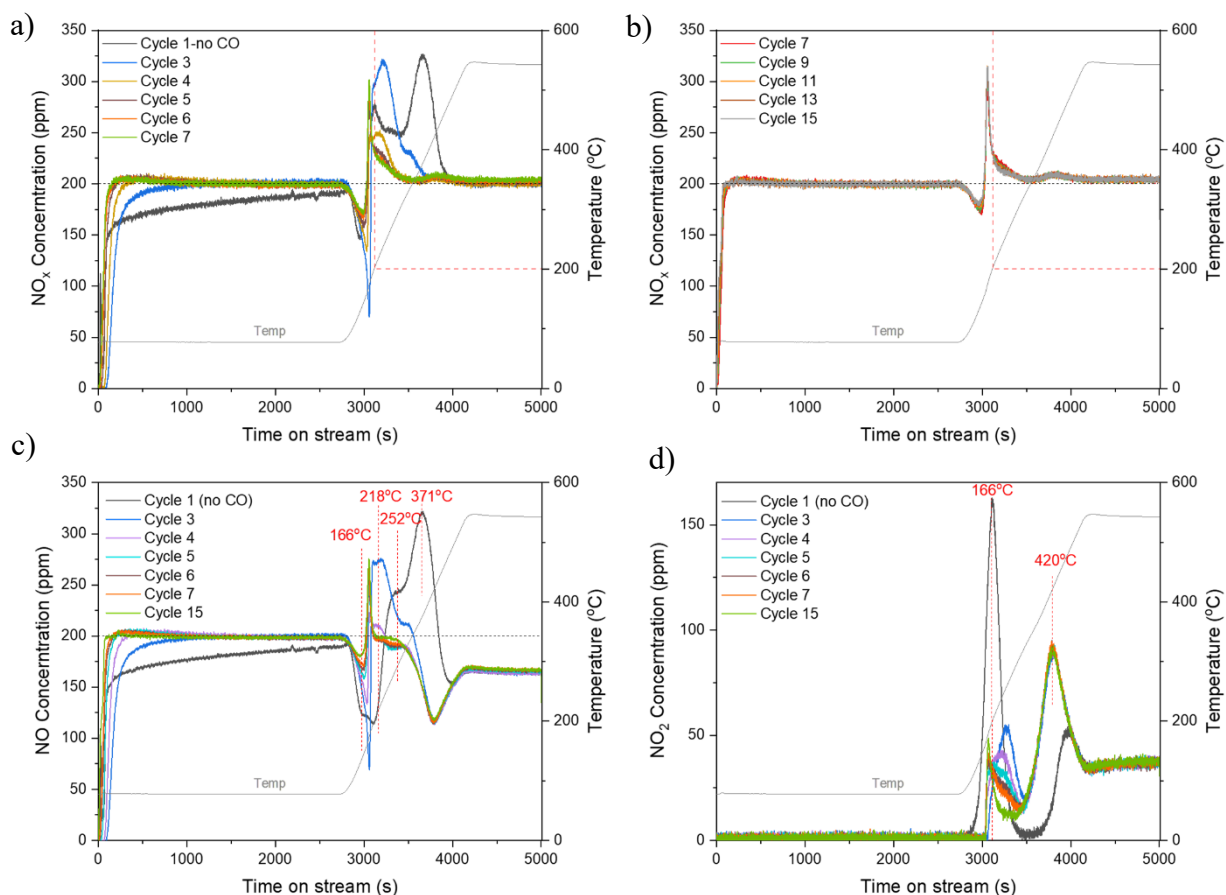


Figure 18. Multi-cycle adsorption and desorption of NO_x using 4000 ppm CO, 200 ppm NO, 8% O₂ and 5% H₂O. (a) and (b) NO_x profiles in Cycles 1-7 and Cycles 7-15, resp., (c) NO and (d) NO₂.

During multiple cycles with high concentrations of CO, $Z^-Pd^{2+}Z^-$ could be reduced to $Z^-H^+ - Pd(0)$ and Z^-H^+ and then be re-oxidized back to $Z^-Pd^{2+}Z^-$. $Z^-H^+ - Pd(0)$ can be one NO adsorption site. In accordance with Ostwald ripening, it was assumed that all Pd(0) sites were converted into Pd(CO)₄¹¹⁴ and, when increasing the temperature thereafter, the Pd(CO)₄ began to release CO and form both active and inactive Pd sites in a more agglomerated form. The active Pd sites adsorbed NO and subsequently released a part of it at temperatures around 218°C. Some of the NO adsorbed on the active Pd sites could be oxidised to form NO₂ at temperatures around 210°C. The active Pd sites were oxidised at higher temperatures and reduced further by NO and CO, which resulted in the consumption of NO at 450°C. Furthermore, the active Pd particles that were produced migrated, and formed larger Pd nanoparticles. Small amounts of NO were adsorbed on the large Pd clusters and partially desorbed at about 200°C. The remaining adsorbed NO was oxidised and formed NO₂ at around 180°C.

5.3 Physicochemical characterisation

Regarding the mechanism proposed for the positive effect of low concentrations of CO, XPS analysis was conducted for degreened Pd/SSZ-13 subjected to two concentrations of CO, i.e. 200 and 400 ppm, and compared with a degreened sample treated without CO. The spectra collected were deconvoluted using Pd²⁺ (337.6 eV(3d_{5/2}) and 342.8 eV (3d_{3/2})) and Pd⁰ (335.9 eV (3d_{5/2}) and 340.6 eV (3d_{3/2})) peaks¹¹⁵⁻¹¹⁷. Fig. 19 shows that no Pd⁰ was present in the absence of CO; for the 200 and 400 ppm CO, amounts of 14% and 59%, respectively, were detected in the XPS deconvolution. This supports the findings of the PNA tests in **Paper III** strongly, wherein it was suggested that the reduction of Pd species is due to the presence of CO in the inlet gas (Section 5.2.1).

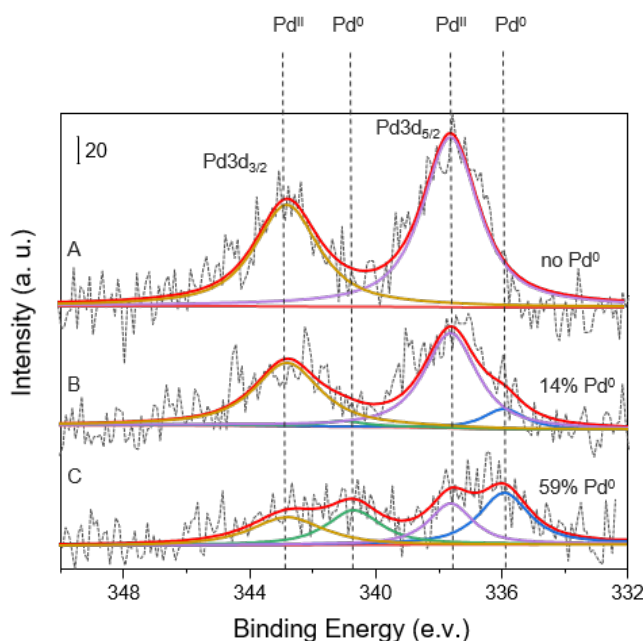


Figure 19. Pd 3d XPS spectra of the Pd/SSZ-13 samples treated at 550°C under the conditions: (A) 200 ppm NO, 5 % H₂O, 8 % O₂ in Ar, (B) 200 ppm NO, 200 ppm CO, 5 % H₂O, 8 % O₂ in Ar and (C) 400 ppm NO, 200 ppm CO, 5 % H₂O, 8 % O₂ in Ar.

In **Paper IV**, the formation of agglomerated Pd clusters was confirmed by STEM-EDX mapping, as shown in Fig. 20. An obvious growth in particle size was detected after exposure to high concentrations of CO after multiple cycles: the particle sizes increased from 6.8 nm to 62 nm on average. As mentioned earlier, this agglomeration is due to Ostwald ripening: particle migration mechanisms occur during the cycles and the formation of Pd(CO)_x starts the Ostwald ripening agglomeration process. In addition, DRIFT spectra were collected during the adsorption of CO on Pd/SSZ-13 both before and after reaction (Fig. 21). The samples were exposed initially to 200 ppm NO, 5% H₂O, 8%O₂ and then 4000 ppm CO was added to

the inlet gas. The formation of nitrate species between $1300\text{-}1700\text{ cm}^{-1}$ ¹¹⁸ was observed first, and thereafter the peaks disappeared in the presence of CO. This shows that the PdO species were reduced by CO and no Pd(NO₃)₂ was formed⁴⁹. Instead, three different peaks appeared in the presence of CO, which were assigned to Pd(CO)_x, Pd-NO and Pd-(NO)(CO) at around 2144, 1816 and 1795 cm⁻¹, respectively. The formation of Pd(CO)_x species in high concentrations of CO was thus confirmed by DRIFT spectroscopy^{47, 119}.

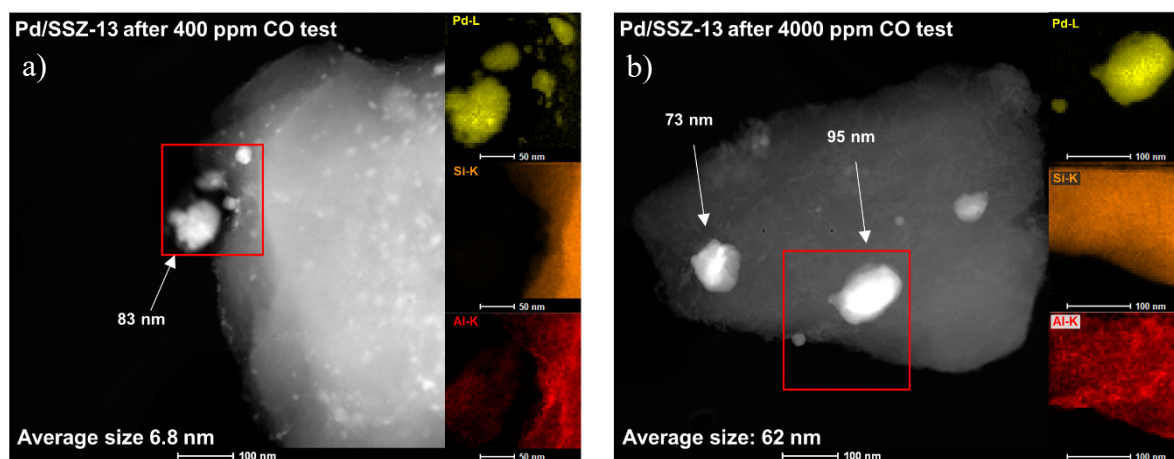


Figure 20. STEM-EDX mapping of Pd/SSZ-13 after exposure to (a) 400 ppm CO PNA test and (b) 4000 ppm CO PNA test.

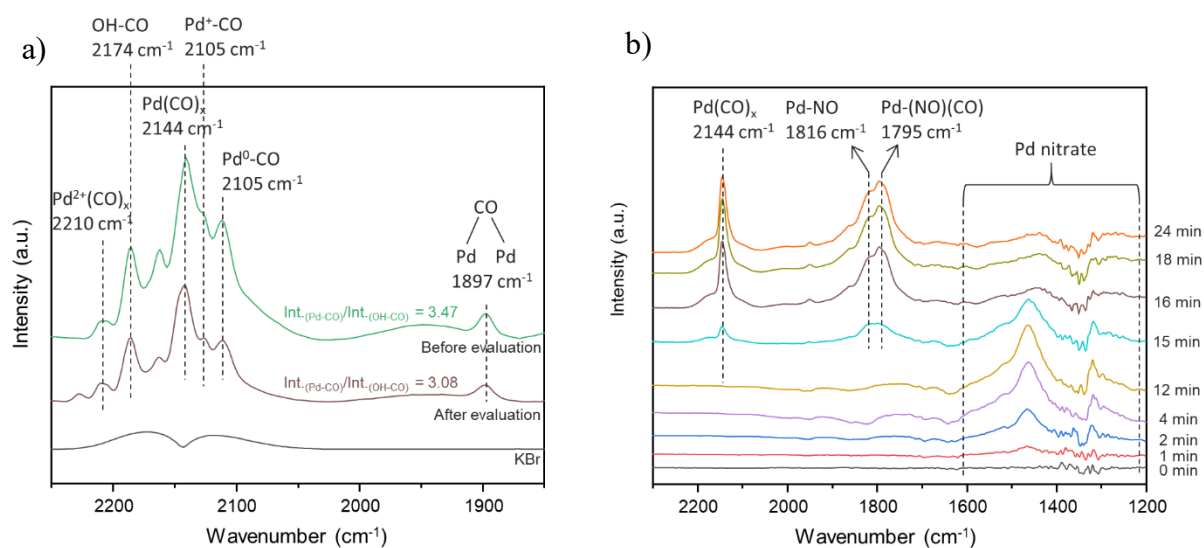


Figure 21. DRIFTS spectra obtained during exposure to (a) 4000 ppm CO at 50°C on Pd/SSZ-13 before and after reaction in flow reactor and (b) 200 ppm NO_x, 4000 ppm CO, 1% H₂O and 8% O₂ at 80°C on fresh Pd/SSZ-13.

Chapter 6

6. The effect of phosphorous poisoning on PNAs

Phosphorous is known to be one of the most severe deactivating compounds in aftertreatment systems^{65,67}. The deactivation mechanism occurs both chemically and physically, which has been found on SCR catalysts^{70, 120-121}. Active sites can be blocked physically by phosphorous and/or both the active sites and the support can react chemically with phosphorous. The effect of phosphorous on Pd/SSZ-13 in passive NO_x adsorption systems was studied in **Paper V**.

6.1 Characterisation of the synthesized Pd/SSZ-13

The synthesised H-SSZ-13 was prepared using the hydrothermal method discussed in Section 3.1.2. ICP-SFMS measurements provided a Si/Al ratio of around 11.5 and a Na content less than 0.05%, which was reported to be sufficient for improving both the hydrothermal stability and catalyst activity¹²²⁻¹²³. The elemental analysis of the calcined Pd/SSZ-13 and the three different concentrations of the phosphorous loading used are given in Table 9, and shows that the presence of phosphorous did not affect the content of palladium in the adsorbents. On the other hand, both the BET surface area and the pore volume of the

Pd/SSZ-13 were decreased when the concentration of phosphorous loading was increased, due to P-poisoning blocking the pores in the Pd/SSZ-13.

Table 9. Elemental analysis, BET surface area and pore volume of the calcined and P-poisoned samples.

Sample	Pd (wt.%)	P (wt.%)	S _{BET} (m ² g ⁻¹)	V _{pore} (g/cm ³)
Pd/SSZ	1.1	-	602.7	0.28
Pd/SSZ-0.4P	1.0	1.3	562.3	0.26
Pd/SSZ-0.6P	1.04	1.5	535.1	0.25
Pd/SSZ-0.8P	1.1	2.6	519.5	0.24

6.2 Physicochemical characterisation

XPS analysis were conducted to provide improved understanding of the effect phosphorous has on Pd/SSZ-13. Fig. 22 shows the P 2P peaks deconvoluted with three phosphorous species: phosphorus pentoxide (P₂O₅, at ~ 135.6 eV), metaphosphate (PO₃⁻, at ~ 134.5 eV) and phosphate (PO₄³⁻ at ~ 133.2 eV)¹²⁴⁻¹²⁵. It was observed that, by increasing the phosphorous content on the Pd/SSZ-13, more metaphosphates and fewer phosphor pentoxides were formed on the adsorbents. Other studies have also confirmed the presence of more PO₃⁻ species at high concentrations of phosphorous on other catalysts^{31, 70, 120, 126}. According to the literature, the formation of P₂O₅ on a catalyst surface can cause physical deactivation by blocking active sites³¹. In addition, the generation of phosphates (PO₃⁻/ PO₄³⁻) can cause chemical deactivation since these species form while phosphorous interacts with active sites and/or the catalyst support^{29, 65, 127}. As the results of XPS (Fig. 22) indicated the presence of both P₂O₅ and PO₃⁻/ PO₄³⁻ species in all of the P-poisoned samples, it can be concluded that phosphorous influenced the Pd/SSZ-13 both chemically and physically. The physical effect of phosphorous was confirmed by the decrease that was reported of both the BET surface area and the pore volume of the P-poisoned samples (Table 9).

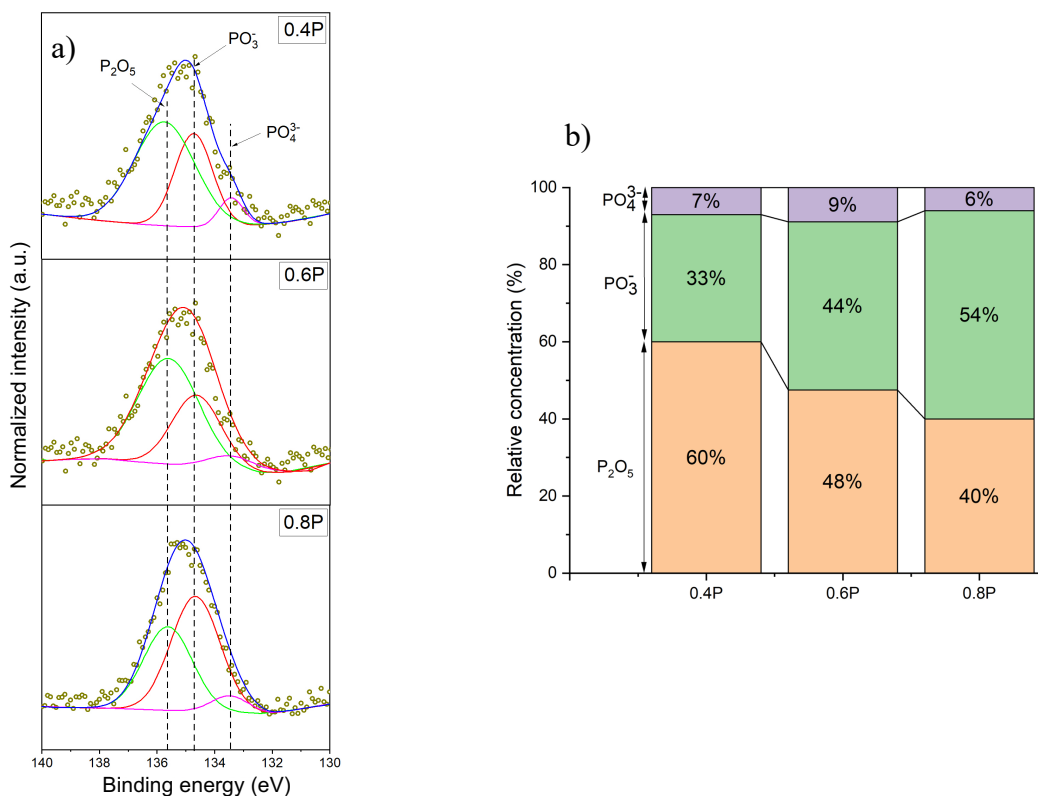


Figure 22. (a) P 2P XP spectra of the degreened 0.4P, 0.6P and 0.8P samples. (b) Corresponding relative concentrations of the phosphorus compounds obtained from spectral deconvolution.

SEM-EDX mapping and ^{27}Al NMR spectra confirmed the chemical deactivation effect of phosphorous on Pd/SSZ-13. Fig. 23a illustrates the EDX mapping of Pd/SSZ-0.4P in which uniform distributions of Al and Si were observed. Several overlapping areas were detected between Pd, P and Al, P and are presented more clearly in the line scan profile in Fig. 23b. These results concur with the literature for the interaction of P with Cu and Al in Cu/SSZ-13⁶⁸. Furthermore, the ^{27}Al NMR spectra of degreened non-poisoned and P-poisoned Pd/SSZ-13 samples showed two main chemical shift signals around 58 and 2 ppm, which were assigned to tetrahedrally-coordinated Al (AlO_4)¹²⁸ and octahedral Al (AlO_6)³⁶ species (Fig. 24). A new signal around δ -12 is observed when introducing phosphorous and it is increasing with increased P loading. This peak was assigned to amorphous Al-O-P species¹²⁹⁻¹³⁰ and is due to dealumination of the zeolite lattice by the reaction with P.

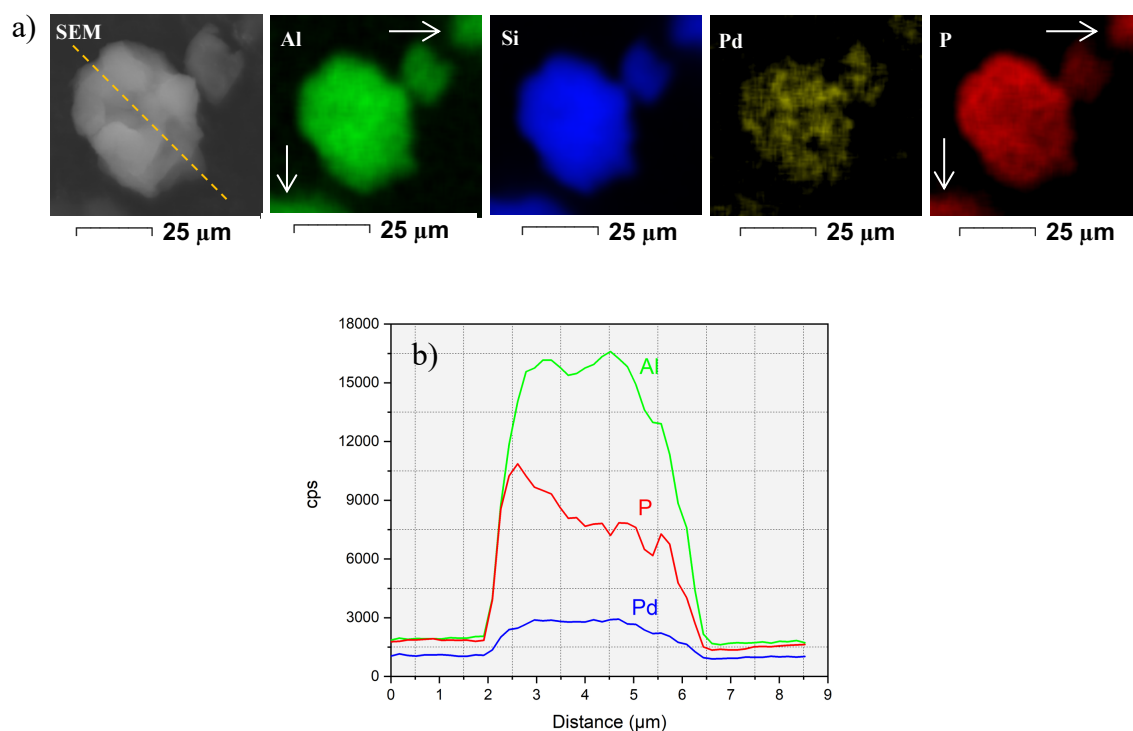


Figure 23. (a) SEM-EDX mapping of Pd/SSZ-0.4P, (b) EDX line scan profiles of Pd, P and Al measured along the dashed line on the top left image.

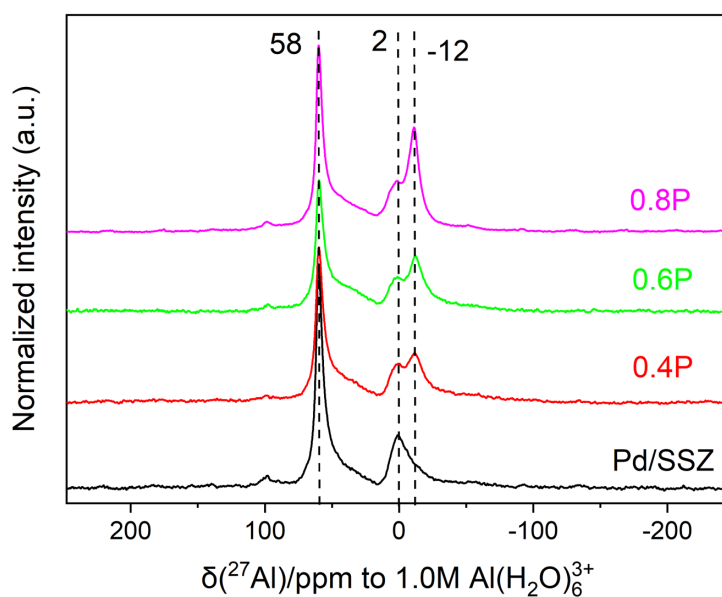


Figure 24. ^{27}Al NMR of the degreened P-poisoned and non-poisoned Pd/SSZ-13. All spectra were normalized according to the weight of the samples.

6.3 DRIFT spectroscopy

In the DRIFTS studies in **Paper V**, two TPD cycles with 200 ppm NO, 1% H_2O and 8% O_2 in Ar were conducted: one with 400 ppm CO and one with none. The adsorption

step was carried out for 15 minutes at 80°C and the following desorption step by ramping up the temperature to 550°C. Fig. 25 displays the peaks related to the Pd nitrates detected around 1317-1523 cm^{-1} ¹¹⁸, which were reduced by increasing the phosphorous content of the Pd/SSZ-13. Whilst the Pd^{2+} ($\text{Pd}^{2+}\text{-NO}$) species around 1861 and 1803 cm^{-1} ^{35, 100} did not lose their intensity in the P-poisoned samples (Fig. 25b). Nitrate peaks could not be detected clearly when CO was present in the adsorption step because the PdO sites were reduced by the CO and fewer $\text{Pd}(\text{NO}_3)_2$ species were formed. Instead, peaks related to $\text{Pd}(\text{CO})_x$, Pd-NO and Pd-(NO)(CO) were detected around 2146, 1860 and 1803 cm^{-1} ^{47, 119}, respectively. The peak around 3730 cm^{-1} , assigned as $\text{Al}^{\text{VI}}(\text{OH})\text{Al}^{\text{VI}}$ bonded to octahedral aluminium, lost intensity by increasing the P-content in Pd/SSZ-13, thereby showing the degrading effect of phosphorous on OH groups. Chen *et al.* reported contamination of OH groups in Pd/zeolite samples in their very recent study²⁹. This illustrates the interaction of phosphorous with the zeolite framework, which concurs with the NMR (Fig. 24) and SEM/EDX mapping (Fig. 25) performed.

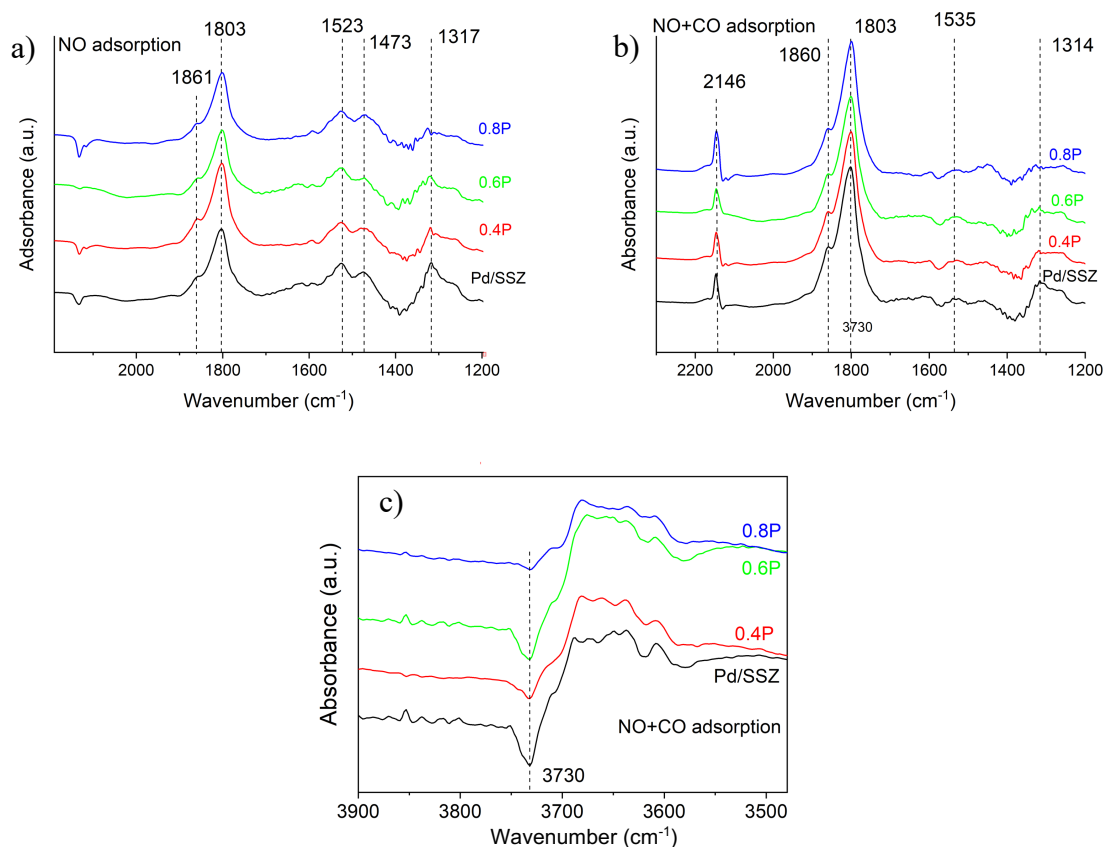


Figure 25. DRIFT spectra obtained with (a) 200 ppm NO, 1% H_2O and 8% O_2 , (b) 400 ppm CO added to the inlet and the spectra presented between 1200 - 2000 cm^{-1} at 80°C and (c) the same gas mixture as (b) but the spectra presented between 3500 - 3900 cm^{-1} at 80°C.

6.4 PNA activity tests

The flow reactor study conducted in **Paper V** had an adsorption step with 200 ppm NO, 8% O₂ and 5% H₂O at 80°C for 2 h, followed by flushing with 8% O₂, 5% H₂O and Ar for 30 minutes. Thereafter, the desorption step began by a temperature increase to 550°C in at a rate of 20°C/min. Fig. 26 illustrates the NO_x desorption profiles of degreened non-poisoned and poisoned samples of Pd/SSZ-13. The main desorption peaks were detected in three different temperature ranges, namely S1: 83-135°C, S2: 136-319°C and S3: 320-438°C. Integration of the profiles of the released NO_x showed a gradual deactivation of Pd/SSZ-13 whilst the phosphorous content was being increased, whereby the desorption of NO_x decreased by 17%, 20% and 31% for 0.4P, 0.6P and 0.8P, respectively. The NO_x/Pd ratio calculated for the three different desorption sites are presented in Table 10, in which the deactivation of the Pd/SSZ-13 by phosphorous can be seen clearly at various desorption sites. This negative effect of phosphorous on catalyst activation has been reported in other studies for Cu/SSZ-13 in NH₃-SCR systems^{68-69, 120}. As mentioned previously, the main species involved in adsorption can be in the form of $Z^-Pd^{2+}Z^-$ or $Z^- [Pd(II)OH]^+$ ^{22, 25}. DRIFT spectroscopy showed adsorbed NO species on these sites by the peaks detected in the area 1800-1880 cm⁻¹. Based on the NO_x/Pd ratio determined (Table 10), which is lower than 1, it can be concluded that PdO_x clusters are also available on the zeolite surface^{25, 47, 50}.

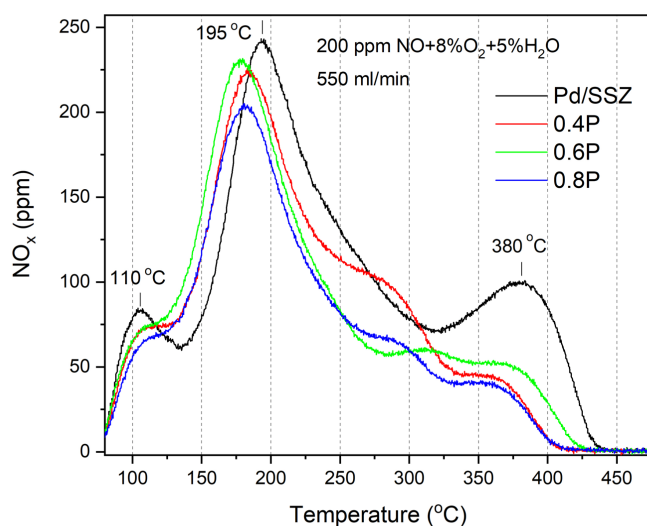


Figure 26. NO_x release profiles of non-poisoned and poisoned Pd/SSZ-13.

Table 10. NO_x/Pd ratios of the non-poisoned and P-poisoned Pd/SSZ-13, where the regions are S1: 83-135°C, S2: 136-319°C and S3: 320-438°C.

<i>Samples</i>	<i>NO_x/Pd Ratio</i>			
	<i>S1</i>	<i>S2</i>	<i>S3</i>	<i>Total</i>
Pd/SSZ	0.08	0.44	0.16	0.68
0.4P	0.06	0.44	0.06	0.56
0.6P	0.05	0.43	0.06	0.54
0.8P	0.04	0.39	0.04	0.47

The desorption profiles of NO and NO₂ during the desorption step in the NO-TPD experiments are given in Fig. 27. Some quantities of PdO species were present on the adsorbent surface, so the NO desorption peak at the lower temperature (S1) can be related to PdO species either by the formation of $Pd(II)NO_3$ or other NO adsorption mechanisms on the clusters of Pd. It was concluded in **Papers III** and **IV** that the NO released at medium temperature is related to the NO on $Z^-Pd^{2+}Z^-$, which can also apply to this study. DRIFT spectroscopy also showed considerable amounts of linear nitrosyl species on Pd/SSZ-13 while adsorbing NO. Additionally, many studies have shown that the $Z^- [Pd(II)OH]^+$ sites can be reduced and adsorb NO with more stable bonds which, in turn, can release NO at higher temperatures^{104, 106}. Low quantities of NO₂ in the inlet flow (~ 3.5 ppm) can be adsorbed on Pd²⁺ and desorbed at lower temperatures; NO oxidation at high temperatures can also form NO₂ at temperatures around 400°C^{50, 71}. Table 10 shows that NO_x desorption at higher temperatures had undergone more reduction after P-poisoning of the Pd/SSZ-13, which indicates that the $Z^- [Pd(II)OH]^+$ sites were affected more drastically by the poisoning process. Moreover, it can be observed in Fig. 27 that the NO₂ released at high temperature was affected by phosphorous poisoning. Presence of less available PdO_x nanoparticles after P-poisoning was evident from O₂-TPD which could explain the lower NO₂ desorption at high temperatures. Less NO₂ release at low temperatures was also due to the presence of less Pd(NO₃)₂ which was shown in the DRIFTS analysis, where fewer nitrates were formed in the poisoned samples. A shift towards lower temperatures for NO₂ indicates a possible change in the binding strength of $[Pd(OH)]^+$. According to the XPS and NMR results, higher concentrations of phosphorous, caused more chemical deactivation of the adsorbent due to interaction of P with either ionic Pd sites or the zeolite framework causing less and less active sites to be available the Pd/SSZ-13 adsorbents.

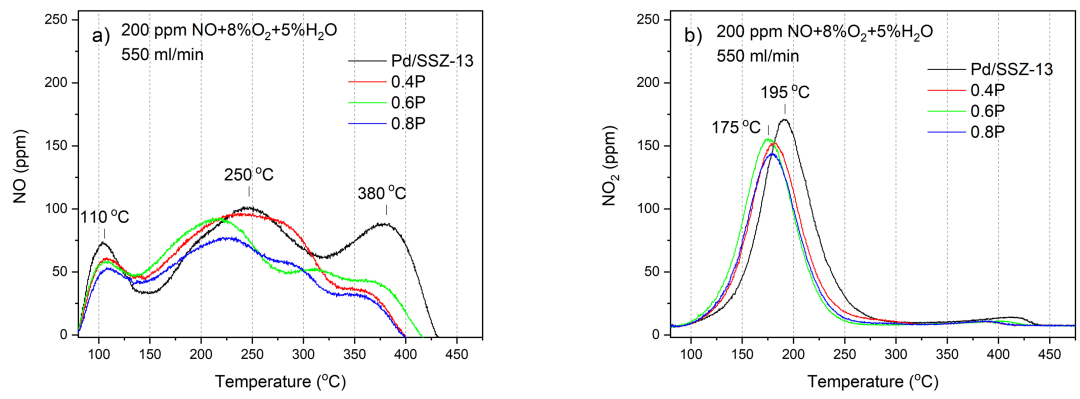


Figure 27. Desorption profiles of the non-poisoned and P-poisoned Pd/SSZ-13 for (a) NO and (b) NO₂.

Chapter 7

7. Conclusions and outlook

The primary aim of this study was to fundamentally study the performance of different Pd/zeolites in passive NO_x adsorption (PNA) processes; for this purpose, the promoters ceria, zirconium and lanthanum were studied first. After observing improvements in the temperature window of NO_x desorption resulting from promotion by La, the effect of different loading concentrations of La was then investigated and compared to the reference sample (Pd/BEA). Thereafter, the study was expanded to investigate the effect of CO on the stability of the performance of the La-promoted Pd/BEA during multiple NO-TPD cycles. Pd/SSZ-13 was used to help comprehend the mechanism for the influences of high and low concentrations of CO and to understand the effect of phosphorous on PNA processes.

Firstly, the study of different promoters indicated that La loading has a remarkable effect on tuning the temperature window of NO_x desorption to values over 200°C whilst Pd/BEA has its maximum desorption peaks at lower temperatures, which is not advantageous for PNA processes. The flow reactor results for various La loadings, ranging from 2.7 wt.% to 10 wt.%, showed 2.7%La-Pd/BEA to have the most favourable temperature range for NO_x desorption. XPS analysis indicated that more Pd²⁺ species were present on the La-modified sample, and DRIFT spectroscopy showed the formation of more nitrates in this sample that required higher temperatures to decompose. Thereafter, the performance stability of Pd-2.7%La/BEA in multiple NO-TPD experiments was investigated with the presence of CO in

high concentrations. The flow reactor results showed a strong degradation behaviour for both the promoted and non-promoted Pd/BEA: 99% of the NO_x released between 200-400°C was lost for Pd/BEA whilst only 64% of the NO_x released was lost in La-promoted samples until the 5th cycle. Degradation ceased after the 5th cycle for Pd-2.7%La/BEA and a more stable behaviour was displayed for this adsorbent until the last step was reached. It was concluded that this deactivation was due to the agglomeration of Pd species during the cycles and the formation of PdO_x clusters on the surface. O₂-TPD showed that significantly higher quantities of PdO_x clusters were formed on the Pd/BEA after multiple cycles with CO compared with the La-modified sample. Fewer active sites were therefore available on Pd/BEA, which caused drastic deactivation. Flow reactor experiments showed that both Pd and La played an important role in the performance stability and release of NO_x from Pd-2.7%La/BEA.

Compared with Pd/BEA, Pd/SSZ-13 showed more beneficial temperature ranges for the release of NO_x in the PNA process. It was concluded that three different Pd sites are involved in the adsorption of NO_x at low temperatures for this adsorbent: $Z^-Pd^{2+}Z^-$, $Z^-[Pd(II)OH]^+$ and PdO, all of which can desorb NO and NO₂ in different temperature ranges. It was observed that low concentrations of CO increased the stability of the NO_x species stored, thus raising the release temperatures above the urea dosing temperature. This was due to the reduction of Pd²⁺ species by the CO and the formation of Pd with lower oxidation states. At high CO concentrations, on the other hand, Pd/SSZ-13 was deactivating in the NO-TPD cycles as a result of sintering and the agglomeration of Pd particles. It was proposed that two Pd sintering modes were involved, namely Ostwald ripening and particle migration. The higher rate of Ostwald ripening sintering meant that the formation of Pd(CO₄) species occurred in the initial NO-TPD cycles; in the later cycles, the active Pd species migrated and formed larger nanoparticles. STEM images showed the formation of larger Pd particles on the adsorbent surface after 15 cycles.

It was also concluded that the adsorption and desorption performances of Pd/zeolites can be affected by phosphorous in PNA processes. The formation of three main phosphorous species, i.e. phosphorus pentoxide (P₂O₅), metaphosphate (PO₃⁻) and phosphate (PO₄³⁻), caused both the chemical and physical deactivation of Pd/SSZ-13. Physical deactivation was caused by the active sites being blocked by phosphorous: smaller surface areas and pore volumes were reported for the P-poisoned samples. NMR and SEM-EDX mapping confirmed that phosphorous reacted with active sites and the zeolite framework by forming Al-O-P species or palladium phosphates.

In this study, it was found that the distribution of palladium on the zeolite plays an important role in the activity of the catalyst: further, and more detailed, understanding can be achieved from research into the various factors that influence the distribution of Pd, along with the investigation of new synthesis techniques. This can be expanded beyond using lanthanum as a promoter on Pd/zeolite, with the aim of improving its adsorption and desorption properties. Acquiring sound knowledge of the P-poisoning mechanism in multiple cycles, and designing a suitable kinetical model to explain the experiments, make for interesting future investigations.

Acknowledgements

This work was performed at The Chemical Engineering and Competence Center of Catalysis. The Swedish Research Council is gratefully acknowledged for their financial support.

I would like to thank:

- My main supervisor, Professor Louise Olsson, for all your encouragement, support and understanding. I am very grateful to have been given the chance of doing my Ph.D. studies in your research group. I was extremely lucky to have a supervisor who cared so much about my work and was always available and supportive in all of the issues and complications that I encountered.
- My co-supervisor and examiner, Derek Creaser, for all your valuable help, discussions and input. It has been such a pleasure having you in my research group.
- Phuoc Hoang Ho and Dawei Yao, for all your support and our many valuable discussions.
- My office colleagues, Jesus, Ida and Dawei, for the amazing discussions and wonderful moments that we experienced every day.
- Stefan Gustafsson and Eric Tam, for your help with TEM and XPS measurements.
- Diana Bernin and Tobias Sparrman for your help with NMR measurements.
- Malin Larsson and Anna Oskarsson for providing administrative support.
- Lasse Urholm and Lennart Norberg for all your help in the reactor labs.
- All my current and former co-workers at KCK for all the fun, discussions and wonderful moments we shared.
- Ghodsieh Isapour, for all the enjoyable and memorable times that we had together.
- All my friends within and outside Chalmers, for being there for me and for all the great times we had.
- Last, but not least, my lovely family and Mohsen. Thank you so much for your never-ending support, and the affection that you show me every moment of my life. I love you more than you will ever know!

References

- (1) Gómez-García, M.; Pitchon, V.; Kiennemann, A. Pollution by nitrogen oxides: an approach to NO_x abatement by using sorbing catalytic materials. *Environment international* **2005**, *31*, 445-467.
- (2) Agency, U. S. E. P. Overview of Greenhouse Gases. <https://www.epa.gov> (accessed 11.March.2020).
- (3) Emission Standards European Union. <https://dieselnet.com/standards/eu/ld.php> (accessed 20.01).
- (4) Arthur, A. J.; Fernandez, G. M., *Supported Metals In Catalysis (2nd Edition)*. World Scientific Publishing Company: 2011.
- (5) Skalska, K.; Miller, J. S.; Ledakowicz, S. Trends in NO_x abatement: A review. *Science of The Total Environment* **2010**, *408*, 3976-3989.
- (6) Ji, Y.; Choi, J.-S.; Toops, T. J.; Crocker, M.; Naseri, M. Influence of ceria on the NO_x storage/reduction behavior of lean NO_x trap catalysts. *Catalysis Today* **2008**, *136*, 146-155.
- (7) Liu, Y.; Harold, M. P.; Luss, D. Coupled NO_x storage and reduction and selective catalytic reduction using dual-layer monolithic catalysts. *Applied Catalysis B: Environmental* **2012**, *121*, 239-251.
- (8) Park, S. M.; Kim, M.-Y.; Kim, E. S.; Han, H.-S.; Seo, G. H₂-SCR of NO on Pt–MnO_x catalysts: Reaction path via NH₃ formation. *Applied Catalysis A: General* **2011**, *395*, 120-128.
- (9) Bosch, H.; Janssen, F., *Catalytic reduction of nitrogen oxides: A review on the fundamentals and technology*. Elsevier: 1988; Vol. 7.
- (10) Fritz, A.; Pitchon, V. The current state of research on automotive lean NO_x catalysis. *Applied Catalysis B: Environmental* **1997**, *13*, 1-25.
- (11) Chiron, M., Effects of Motor Vehicle Pollutants on Health. In *Studies in Surface Science and Catalysis*, Crucq, A.; Frennet, A., Eds. Elsevier: 1987; Vol. 30, pp 1-10.
- (12) Epling, W. S.; Campbell, L. E.; Yezerets, A.; Currier, N. W.; Parks, J. E. Overview of the Fundamental Reactions and Degradation Mechanisms of NO_x Storage/Reduction Catalysts. *Catalysis Reviews* **2004**, *46*, 163-245.
- (13) Bailey, D.; Solomon, G. Pollution prevention at ports: clearing the air. *Environmental impact assessment review* **2004**, *24*, 749-774.
- (14) Blaszczyk, R.; Cox, L.; Clean Air Technology, C., *Nitrogen oxides (NO_x) : why and how they are controlled*. U.S. Environmental Protection Agency, Office of Air Quality Planning and Standards, Information Transfer and Program Integration Division, Clean Air Technology Center: Research Triangle Park, N.C., 1999.
- (15) Beale, A. M.; Gao, F.; Lezcano-Gonzalez, I.; Peden, C. H.; Szanyi, J. Recent advances in automotive catalysis for NO_x emission control by small-pore microporous materials. *Chemical Society Reviews* **2015**, *44*, 7371-7405.
- (16) Forzatti, P.; Nova, I.; Tronconi, E. New “Enhanced NH₃-SCR” Reaction for NO_x Emission Control. *Industrial & Engineering Chemistry Research* **2010**, *49*, 10386-10391.
- (17) Jones, S.; Ji, Y.; Bueno-Lopez, A.; Song, Y.; Crocker, M. CeO₂-M₂O₃ Passive NO_x Adsorbers for Cold Start Applications. *Emission Control Science and Technology* **2017**, *3*, 59-72.
- (18) Jones, S.; Ji, Y.; Crocker, M. Ceria-based Catalysts for Low Temperature NO_x storage and Release. *Catalysis Letters* **2016**, *146*, 909-917.
- (19) Fridell, E.; Persson, H.; Westerberg, B.; Olsson, L.; Skoglundh, M. The mechanism for NO_x storage. *Catalysis Letters* **2000**, *66*, 71-74.
- (20) Mahzoul, H.; Brillhac, J. F.; Gilot, P. Experimental and mechanistic study of NO_x adsorption over NO_x trap catalysts. *Applied Catalysis B: Environmental* **1999**, *20*, 47-55.

- (21) Mihai, O.; Trandafilović, L.; Wentworth, T.; Torres, F. F.; Olsson, L. The Effect of Si/Al Ratio for Pd/BEA and Pd/SSZ-13 Used as Passive NO_x Adsorbers. *Topics in Catalysis* **2018**, *61*, 2007-2020.
- (22) Chen, H.-Y.; Collier, J. E.; Liu, D.; Mantarosie, L.; Durán-Martín, D.; Novák, V.; Rajaram, R. R.; Thompsett, D. Low Temperature NO Storage of Zeolite Supported Pd for Low Temperature Diesel Engine Emission Control. *Catalysis Letters* **2016**, *146*, 1706-1711.
- (23) Ren, S.; Schmieg, S. J.; Koch, C. K.; Qi, G.; Li, W. Investigation of Ag-based low temperature NO_x adsorbers. *Catalysis Today* **2015**, *258*, 378-385.
- (24) Ji, Y.; Bai, S.; Crocker, M. Al₂O₃-based passive NO_x adsorbers for low temperature applications. *Applied Catalysis B: Environmental* **2015**, *170*, 283-292.
- (25) Zheng, Y.; Kovarik, L.; Engelhard, M. H.; Wang, Y.; Wang, Y.; Gao, F.; Szanyi, J. Low-Temperature Pd/Zeolite Passive NO_x Adsorbers: Structure, Performance, and Adsorption Chemistry. *The Journal of Physical Chemistry C* **2017**, *121*, 15793-15803.
- (26) Vu, A.; Luo, J.; Li, J.; Epling, W. S. Effects of CO on Pd/BEA Passive NO_x Adsorbers. *Catalysis Letters* **2017**, *147*, 745-750.
- (27) Yuntao Gu, R. P. Z., Yu-Ren Chen, William S. Epling Investigation of an irreversible NO_x storage degradation Mode on a Pd/BEA passive NO_x adsorber. *Applied Catalysis B: Environmental* **2019**, *258*, 118032.
- (28) Theis, J. R.; Ura, J. A. Assessment of Zeolite-Based Low Temperature NO_x Adsorbers: Effect of Reductants During Multiple Sequential Cold Starts. *Catalysis Today* **2020**.
- (29) Chen, D.; Lei, H.; Xiong, W.; Li, Y.; Ji, X.; Yang, J.-Y.; Peng, B.; Fu, M.; Chen, P.; Ye, D. Unravelling Phosphorus-Induced Deactivation of Pd-SSZ-13 for Passive NO_x Adsorption and CO Oxidation. *ACS Catalysis* **2021**, *11*, 13891-13901.
- (30) Xie, K.; Wang, A.; Woo, J.; Kumar, A.; Kamasamudram, K.; Olsson, L. Deactivation of Cu-SSZ-13 SCR catalysts by vapor-phase phosphorus exposure. *Applied Catalysis B: Environmental* **2019**, *256*, 117815.
- (31) Wang, A.; Xie, K.; Bernin, D.; Kumar, A.; Kamasamudram, K.; Olsson, L. Deactivation mechanism of Cu active sites in Cu/SSZ-13 — Phosphorus poisoning and the effect of hydrothermal aging. *Applied Catalysis B: Environmental* **2020**, *269*, 118781.
- (32) Xie, K.; Leistner, K.; Wijayanti, K.; Kumar, A.; Kamasamudram, K.; Olsson, L. Influence of phosphorus on Cu-SSZ-13 for selective catalytic reduction of NO_x by ammonia. *Catalysis Today* **2017**, *297*, 46-52.
- (33) Gu, Y.; Epling, W. S. Passive NO_x adsorber: An overview of catalyst performance and reaction chemistry. *Applied Catalysis A: General* **2019**, *570*, 1-14.
- (34) Chen, H.-Y.; Mulla, S.; Weigert, E.; Camm, K.; Ballinger, T.; Cox, J.; Blakeman, P. Cold Start Concept (CSCTM) A Novel Catalyst for Cold Start Emission Control. *SAE International Journal of Fuels and Lubricants* **2013**, *6*, 372-381.
- (35) Ryou, Y.; Lee, J.; Cho, S. J.; Lee, H.; Kim, C. H.; Kim, D. H. Activation of Pd/SSZ-13 catalyst by hydrothermal aging treatment in passive NO adsorption performance at low temperature for cold start application. *Applied Catalysis B: Environmental* **2017**, *212*, 140-149.
- (36) Ryou, Y.; Lee, J.; Lee, H.; Kim, C. H.; Kim, D. H. Effect of various activation conditions on the low temperature NO adsorption performance of Pd/SSZ-13 passive NO_x adsorber. *Catalysis Today* **2019**, *320*, 175-180.
- (37) Lee, J.; Ryou, Y.; Cho, S. J.; Lee, H.; Kim, C. H.; Kim, D. H. Investigation of the active sites and optimum Pd/Al of Pd/ZSM-5 passive NO adsorbers for the cold-start application: Evidence of isolated-Pd species obtained after a high-temperature thermal treatment. *Applied Catalysis B: Environmental* **2018**, *226*, 71-82.
- (38) Ryou, Y.; Lee, J.; Lee, H.; Kim, C. H.; Kim, D. H. Low temperature NO adsorption over hydrothermally aged Pd/CeO₂ for cold start application. *Catalysis Today* **2018**, *307*, 93-101.

- (39) Theis, J. R. An assessment of Pt and Pd model catalysts for low temperature NO_x adsorption. *Catalysis Today* **2016**, 267, 93-109.
- (40) Ji, Y.; Xu, D.; Bai, S.; Graham, U.; Crocker, M.; Chen, B.; Shi, C.; Harris, D.; Scapens, D.; Darab, J. Pt- and Pd-Promoted CeO₂-ZrO₂ for Passive NO_x Adsorber Applications. *Industrial & Engineering Chemistry Research* **2017**, 56, 111-125.
- (41) Umeno, T.; Hanzawa, M.; Hayashi, Y.; Hori, M., Development of New Lean NO_x Trap Technology with High Sulfur Resistance. SAE International: 2014.
- (42) Chang, X.; Lu, G.; Guo, Y.; Wang, Y.; Guo, Y. A high effective adsorbent of NO_x: Preparation, characterization and performance of Ca-beta zeolites. *Microporous and Mesoporous Materials* **2013**, 165, 113-120.
- (43) Murata, Y.; Morita, T.; Wada, K.; Ohno, H. NO_x Trap Three-Way Catalyst (N-TWC) Concept TWC with NO_x Adsorption Properties at Low Temperatures for Cold-Start Emission Control. *SAE International Journal of Fuels and Lubricants* **2015**, 8, 454-459.
- (44) Villamaina, R.; Iacobone, U.; Nova, I.; Tronconi, E.; Ruggeri, M. P.; Mantarosie, L.; Collier, J.; Thompsett, D. Mechanistic insight in NO trapping on Pd/Chabazite systems for the low-temperature NO_x removal from Diesel exhausts. *Applied Catalysis B: Environmental* **2021**, 284, 119724.
- (45) Ogura, M.; Hayashi, M.; Kage, S.; Matsukata, M.; Kikuchi, E. Determination of active palladium species in ZSM-5 zeolite for selective reduction of nitric oxide with methane. *Applied Catalysis B: Environmental* **1999**, 23, 247-257.
- (46) Aylor, A. W.; Lobree, L. J.; Reimer, J. A.; Bell, A. T. Investigations of the Dispersion of Pd in H-ZSM-5. *Journal of Catalysis* **1997**, 172, 453-462.
- (47) Khivantsev, K.; Gao, F.; Kovarik, L.; Wang, Y.; Szanyi, J. Molecular Level Understanding of How Oxygen and Carbon Monoxide Improve NO_x Storage in Palladium/SSZ-13 Passive NO_x Adsorbers: The Role of NO⁺ and Pd(II)(CO)(NO) Species. *The Journal of Physical Chemistry C* **2018**, 122, 10820-10827.
- (48) Adelman, B. J.; Sachtler, W. M. H. The effect of zeolitic protons on NO_x reduction over Pd/ZSM-5 catalysts. *Applied Catalysis B: Environmental* **1997**, 14, 1-11.
- (49) Yao, D.; Feizie Ilmasani, R.; Wurzenberger, J. C.; Glatz, T.; Han, J.; Wang, A.; Creaser, D.; Olsson, L. Kinetic modeling of CO assisted passive NO_x adsorption on Pd/SSZ-13. *Chemical Engineering Journal* **2022**, 428, 132459.
- (50) Wang, A.; Lindgren, K.; Di, M.; Bernin, D.; Carlsson, P.-A.; Thuvander, M.; Olsson, L. Insight into hydrothermal aging effect on Pd sites over Pd/LTA and Pd/SSZ-13 as PNA and CO oxidation monolith catalysts. *Applied Catalysis B: Environmental* **2020**, 278, 119315.
- (51) Schmeisser, V.; Weibel, M.; Sebastian Hernando, L.; Nova, I.; Tronconi, E.; Ruggeri, M. P., Cold Start Effect Phenomena over Zeolite SCR Catalysts for Exhaust Gas Aftertreatment. SAE International: 2013.
- (52) Gao, F.; Wang, Y.; Kollár, M.; Washton, N. M.; Szanyi, J.; Peden, C. H. F. A comparative kinetics study between Cu/SSZ-13 and Fe/SSZ-13 SCR catalysts. *Catalysis Today* **2015**, 258, 347-358.
- (53) Mihai, O.; Trandafilović, L.; Wentworth, T.; Torres, F. F.; Olsson, L. The Effect of Si/Al Ratio for Pd/BEA and Pd/SSZ-13 Used as Passive NO_x Adsorbers. *Topics in Catalysis* **2018**, 61, 2007-2020.
- (54) Porta, A.; Pellegrinelli, T.; Castoldi, L.; Matarrese, R.; Morandi, S.; Dzwigaj, S.; Lietti, L. Low Temperature NO_x Adsorption Study on Pd-Promoted Zeolites. *Topics in Catalysis* **2018**, 61, 2021-2034.
- (55) Li, W. B.; Yang, X. F.; Chen, L. F.; Wang, J. A. Adsorption/desorption of NO_x on MnO₂/ZrO₂ oxides prepared in reverse microemulsions. *Catalysis Today* **2009**, 148, 75-80.

- (56) Theis, J. R.; Lambert, C. The Effects of CO, C₂H₄, and H₂O on the NO_x Storage Performance of Low Temperature NO_x Adsorbers for Diesel Applications. *SAE International Journal of Engines* **2017**, *10*, 1627-1637.
- (57) Mei, D.; Gao, F.; Szanyi, J.; Wang, Y. Mechanistic insight into the passive NO_x adsorption in the highly dispersed Pd/HBEA zeolite. *Applied Catalysis A: General* **2019**, *569*, 181-189.
- (58) Okumura, K.; Amano, J.; Yasunobu, N.; Niwa, M. X-ray Absorption Fine Structure Study of the Formation of the Highly Dispersed PdO over ZSM-5 and the Structural Change of Pd Induced by Adsorption of NO. *The Journal of Physical Chemistry B* **2000**, *104*, 1050-1057.
- (59) Tew, M. W.; Miller, J. T.; van Bokhoven, J. A. Particle size effect of hydride formation and surface hydrogen adsorption of nanosized palladium catalysts: L3 edge vs K edge X-ray absorption spectroscopy. *The Journal of Physical Chemistry C* **2009**, *113*, 15140-15147.
- (60) Nag, N. K. A study on the formation of palladium hydride in a carbon-supported palladium catalyst. *The Journal of Physical Chemistry B* **2001**, *105*, 5945-5949.
- (61) Ryou, Y.; Lee, J.; Lee, H.; Kim, C. H.; Kim, D. H. Effect of sulfur aging and regeneration on low temperature NO adsorption over hydrothermally treated Pd/CeO₂ and Pd/Ce_{0.58}Zr_{0.42}O₂ catalysts. *Catalysis Today* **2017**, *297*, 53-59.
- (62) Bodek, K. M.; Wong, V. V. The Effects of Sulfated Ash, Phosphorus and Sulfur on Diesel Aftertreatment Systems-A Review. **2007**.
- (63) Forzatti, P.; Lietti, L.; Tronconi, E. Nitrogen oxides removal—industrial. *Encyclopedia of Catalysis* **2002**.
- (64) Selleri, T.; Melas, A. D.; Joshi, A.; Manara, D.; Perujo, A.; Suarez-Bertoa, R. An overview of lean exhaust denox aftertreatment technologies and NO_x emission regulations in the european union. *Catalysts* **2021**, *11*, 404.
- (65) Eaton, S. J.; Bunting, B. G.; Toops, T. J., The Roles of Phosphorus and Soot on the Deactivation of Diesel Oxidation Catalysts. SAE International: 2009.
- (66) Lee, J.; Theis, J. R.; Kyriakidou, E. A. Vehicle emissions trapping materials: Successes, challenges, and the path forward. *Applied Catalysis B: Environmental* **2019**, *243*, 397-414.
- (67) Väliheikki, A.; Kärkkäinen, M.; Honkanen, M.; Heikkinen, O.; Kolli, T.; Kallinen, K.; Huuhtanen, M.; Vippola, M.; Lahtinen, J.; Keiski, R. L. Deactivation of Pt/SiO₂-ZrO₂ diesel oxidation catalysts by sulphur, phosphorus and their combinations. *Applied Catalysis B: Environmental* **2017**, *218*, 409-419.
- (68) Xie, K.; Woo, J.; Bernin, D.; Kumar, A.; Kamasamudram, K.; Olsson, L. Insights into hydrothermal aging of phosphorus-poisoned Cu-SSZ-13 for NH₃-SCR. *Applied Catalysis B: Environmental* **2019**, *241*, 205-216.
- (69) Wang, A.; Wang, J.; Sheti, S.; Dahlin, S.; Han, J.; Woo, J.; Xie, K.; Pettersson, L. J.; Olsson, L. A deactivation mechanism study of phosphorus-poisoned diesel oxidation catalysts: model and supplier catalysts. *Catalysis Science & Technology* **2020**, *10*, 5602-5617.
- (70) Rokosz, M. J.; Chen, A. E.; Lowe-Ma, C. K.; Kucherov, A. V.; Benson, D.; Paputa Peck, M. C.; McCabe, R. W. Characterization of phosphorus-poisoned automotive exhaust catalysts. *Applied Catalysis B: Environmental* **2001**, *33*, 205-215.
- (71) Wang, A.; Xie, K.; Kumar, A.; Kamasamudram, K.; Olsson, L. Layered Pd/SSZ-13 with Cu/SSZ-13 as PNA – SCR dual-layer monolith catalyst for NO_x abatement. *Catalysis Today* **2020**.
- (72) Deka, U.; Juhin, A.; Eilertsen, E. A.; Emerich, H.; Green, M. A.; Korhonen, S. T.; Weckhuysen, B. M.; Beale, A. M. Confirmation of isolated Cu²⁺ ions in SSZ-13 zeolite as active sites in NH₃-selective catalytic reduction. *The Journal of Physical Chemistry C* **2012**, *116*, 4809-4818.
- (73) Gao, F.; Washton, N. M.; Wang, Y.; Kollár, M.; Szanyi, J.; Peden, C. H. F. Effects of Si/Al ratio on Cu/SSZ-13 NH₃-SCR catalysts: Implications for the active Cu species and the roles of Brønsted acidity. *Journal of Catalysis* **2015**, *331*, 25-38.

- (74) Azis, M. M., *Experimental and kinetic studies of H₂ effect on lean exhaust aftertreatment processes : HC-SCR and DOC*. Chalmers University of Technology: 2015.
- (75) Yasumura, S.; Ide, H.; Ueda, T.; Jing, Y.; Liu, C.; Kon, K.; Toyao, T.; Maeno, Z.; Shimizu, K.-i. Transformation of Bulk Pd to Pd Cations in Small-Pore CHA Zeolites Facilitated by NO. *JACS Au* **2021**, *1*, 201-211.
- (76) Brunauer, S.; Emmett, P. H.; Teller, E. Adsorption of Gases in Multimolecular Layers. *Journal of the American Chemical Society* **1938**, *60*, 309-319.
- (77) Leofanti, G.; Padovan, M.; Tozzola, G.; Venturelli, B. Surface area and pore texture of catalysts. *Catalysis Today* **1998**, *41*, 207-219.
- (78) Süheyda Atalay, G. E., *Novel Catalysts in Advanced Oxidation of Organic Pollutants*. 1st ed. 2016. ed.; Springer eBooks: 2016.
- (79) Beller, M.; Renken, A.; Santen, R. A. v., *Catalysis : from principles to applications*. Wiley-VCH: 2012.
- (80) Carter, C. B.; Williams, D. B., *Transmission Electron Microscopy. [electronic resource] : Diffraction, Imaging, and Spectrometry*. 1st ed. 2016. ed.; Springer International Publishing: 2016.
- (81) van der Heide, P., *X-ray Photoelectron Spectroscopy : An introduction to Principles and Practices*. 1st ed. ed.; Wiley: 2011.
- (82) Kulprathipanja, S., 6. Aspects of Mechanisms, Processes, and Requirements for Zeolite Separation. John Wiley & Sons: 2017.
- (83) Arunagiri, T.; Golden, T. D.; Chyan, O. Study of palladium metal particle deposition on the conductive diamond surface by XRD, XPS and electrochemistry. *Materials Chemistry and Physics* **2005**, *92*, 152-158.
- (84) Leskes, M., Nuclear Magnetic Resonance Spectroscopy | Solid-State☆. In *Encyclopedia of Analytical Science (Third Edition)*, Worsfold, P.; Poole, C.; Townshend, A.; Miró, M., Eds. Academic Press: Oxford, 2019; pp 403-413.
- (85) Nowacka, A., *Polarization transfer solid-state NMR for studying soft matter: From surfactants to the stratum corneum*. Lund University: 2012.
- (86) Chorkendorff, I.; Niemantsverdriet, J. W., *Concepts of modern catalysis and kinetics*. 2nd, rev. and enlarged ed. ed.; Wiley-VCH: 2007.
- (87) Hoost, T.; Otto, K. Temperature-programmed study of the oxidation of palladium/alumina catalysts and their lanthanum modification. *Applied Catalysis A: General* **1992**, *92*, 39-58.
- (88) Weast, R. C.; Astle, M. J.; Beyer, W. H., *CRC handbook of chemistry and physics*. CRC press Boca Raton, FL: 1988; Vol. 69.
- (89) Yu, Y.; Takei, T.; Ohashi, H.; He, H.; Zhang, X.; Haruta, M. Pretreatments of Co₃O₄ at moderate temperature for CO oxidation at -80°C. *Journal of Catalysis* **2009**, *267*, 121-128.
- (90) Lou, Y.; Ma, J.; Hu, W.; Dai, Q.; Wang, L.; Zhan, W.; Guo, Y.; Cao, X.-M.; Guo, Y.; Hu, P.; Lu, G. Low-Temperature Methane Combustion over Pd/H-ZSM-5: Active Pd Sites with Specific Electronic Properties Modulated by Acidic Sites of H-ZSM-5. *ACS Catalysis* **2016**, *6*, 8127-8139.
- (91) Simplício, L. M. T.; Brandão, S. T.; Sales, E. A.; Lietti, L.; Bozon-Verduraz, F. Methane combustion over PdO-alumina catalysts: The effect of palladium precursors. *Applied Catalysis B: Environmental* **2006**, *63*, 9-14.
- (92) Buzková Arvajová, A.; Boutikos, P.; Pečinka, R.; Kočí, P. Global kinetic model of NO oxidation on Pd/γ-Al₂O₃ catalyst including PdO_x formation and reduction by CO and C₃H₆. *Applied Catalysis B: Environmental* **2020**, *260*, 118141.
- (93) Ryou, Y.; Lee, J.; Kim, Y.; Hwang, S.; Lee, H.; Kim, C. H.; Kim, D. H. Effect of reduction treatments (H₂ vs. CO) on the NO adsorption ability and the physicochemical properties of Pd/SSZ-13 passive NO_x adsorber for cold start application. *Applied Catalysis A: General* **2019**, *569*, 28-34.

- (94) Hess, C.; Ozensoy, E.; Yi, C.-W.; Goodman, D. W. NO Dimer and Dinitrosyl Formation on Pd(111): From Ultra-High-Vacuum to Elevated Pressure Conditions. *Journal of the American Chemical Society* **2006**, *128*, 2988-2994.
- (95) Sedlmair, C.; Gil, B.; Seshan, K.; Jentys, A.; Lercher, J. A. An in situ IR study of the NO_x adsorption/reduction mechanism on modified Y zeolites. *Physical Chemistry Chemical Physics* **2003**, *5*, 1897-1905.
- (96) Hadjiivanov, K. Use of overtones and combination modes for the identification of surface NO_x anionic species by IR spectroscopy. *Catalysis Letters* **2000**, *68*, 157-161.
- (97) Meunier, F.; Zuzaniuk, V.; Breen, J.; Olsson, M.; Ross, J. Mechanistic differences in the selective reduction of NO by propene over cobalt-and silver-promoted alumina catalysts: kinetic and in situ DRIFTS study. *Catalysis Today* **2000**, *59*, 287-304.
- (98) Westerberg, B.; Fridell, E. A transient FTIR study of species formed during NO_x storage in the Pt/BaO/Al₂O₃ system. *Journal of Molecular Catalysis A: Chemical* **2001**, *165*, 249-263.
- (99) Kim, Y.; Hwang, S.; Lee, J.; Ryou, Y.; Lee, H.; Kim, C. H.; Kim, D. H. Comparison of NO_x Adsorption/Desorption Behaviors over Pd/CeO₂ and Pd/SSZ-13 as Passive NO_x Adsorbers for Cold Start Application. *Emission Control Science and Technology* **2019**, *5*, 172-182.
- (100) Khivantsev, K.; Jaegers, N. R.; Kovarik, L.; Hanson, J. C.; Tao, F.; Tang, Y.; Zhang, X.; Koleva, I. Z.; Aleksandrov, H. A.; Vayssilov, G. N.; Wang, Y.; Gao, F.; Szanyi, J. Achieving Atomic Dispersion of Highly Loaded Transition Metals in Small-Pore Zeolite SSZ-13: High-Capacity and High-Efficiency Low-Temperature CO and Passive NO_x Adsorbers. *Angewandte Chemie International Edition* **2018**, *57*, 16672-16677.
- (101) Zhu, H.; Qin, Z.; Shan, W.; Shen, W.; Wang, J. Pd/CeO₂-TiO₂ catalyst for CO oxidation at low temperature: a TPR study with H₂ and CO as reducing agents. *Journal of Catalysis* **2004**, *225*, 267-277.
- (102) Wang, X.; Chen, H.; Sachtler, W. M. H. Selective reduction of NO_x with hydrocarbons over Co/MFI prepared by sublimation of CoBr₂ and other methods. *Applied Catalysis B: Environmental* **2001**, *29*, 47-60.
- (103) Gupta, A.; Kang, S. B.; Harold, M. P. NO_x uptake and release on Pd/SSZ-13: Impact Of Feed composition and temperature. *Catalysis Today* **2020**.
- (104) Ambast, M.; Karinshak, K.; Rahman, B. M. M.; Grabow, L. C.; Harold, M. P. Passive NO_x Adsorption on Pd/H-ZSM-5: Experiments and Modeling. *Applied Catalysis B: Environmental* **2020**, 118802.
- (105) Descorme, C.; Gélin, P.; Primet, M.; Lécuyer, C. Infrared study of nitrogen monoxide adsorption on palladium ion-exchanged ZSM-5 catalysts. *Catalysis Letters* **1996**, *41*, 133-138.
- (106) Mandal, K.; Gu, Y.; Westendorff, K. S.; Li, S.; Pihl, J. A.; Grabow, L. C.; Epling, W. S.; Paolucci, C. Condition-Dependent Pd Speciation and NO Adsorption in Pd/Zeolites. *ACS Catalysis* **2020**, *10*, 12801-12818.
- (107) Sasmaz, E.; Wang, C.; Lance, M. J.; Lauterbach, J. In situ spectroscopic investigation of a Pd local structure over Pd/CeO₂ and Pd/MnO_x-CeO₂ during CO oxidation. *Journal of Materials Chemistry A* **2017**, *5*, 12998-13008.
- (108) Hansen, T. W.; DeLaRiva, A. T.; Challa, S. R.; Datye, A. K. Sintering of catalytic nanoparticles: particle migration or Ostwald ripening? *Accounts of Chemical Research* **2013**, *46*, 1720-1730.
- (109) Ouyang, R.; Liu, J.-X.; Li, W.-X. Atomistic theory of Ostwald ripening and disintegration of supported metal particles under reaction conditions. *Journal of the American Chemical Society* **2013**, *135*, 1760-1771.
- (110) Parkinson, G. S.; Novotny, Z.; Argentero, G.; Schmid, M.; Pavelec, J.; Kosak, R.; Blaha, P.; Diebold, U. Carbon monoxide-induced adatom sintering in a Pd-Fe₃O₄ model catalyst. *Nature Materials* **2013**, *12*, 724-728.

- (111) Zheng, J. W.; Zhou, J. F.; Lin, H. Q.; Duan, X. P.; Williams, C. T.; Yuan, Y. Z. CO-Mediated Deactivation Mechanism of SiO₂-Supported Copper Catalysts during Dimethyl Oxalate Hydrogenation to Ethylene Glycol. *Journal Of Physical Chemistry C* **2015**, *119*, 13758-13766.
- (112) Challa, S. R.; Delariva, A. T.; Hansen, T. W.; Helveg, S.; Sehested, J.; Hansen, P. L.; Garzon, F.; Datye, A. K. Relating rates of catalyst sintering to the disappearance of individual nanoparticles during Ostwald ripening. *Journal of the American Chemical Society* **2011**, *133*, 20672-20675.
- (113) Liu, L.; Lopez-Haro, M.; Lopes, C. W.; Li, C.; Concepcion, P.; Simonelli, L.; Calvino, J. J.; Corma, A. Regioselective generation and reactivity control of subnanometric platinum clusters in zeolites for high-temperature catalysis. *Nat Mater* **2019**, *18*, 866-873.
- (114) Li, J.; Schreckenbach, G.; Ziegler, T. A reassessment of the first metal-carbonyl dissociation energy in M (CO)₄ (M= Ni, Pd, Pt), M (CO)₅ (M= Fe, Ru, Os), and M (CO)₆ (M= Cr, Mo, W) by a quasirelativistic density functional method. *Journal of the American Chemical Society* **1995**, *117*, 486-494.
- (115) Li, Y.; Yu, Y.; Wang, J.-G.; Song, J.; Li, Q.; Dong, M.; Liu, C.-J. CO oxidation over graphene supported palladium catalyst. *Applied Catalysis B: Environmental* **2012**, *125*, 189-196.
- (116) Ivanova, A. S.; Slavinskaya, E. M.; Gulyaev, R. V.; Zaikovskii, V. I.; Stonkus, O.; Danilova, I. G.; Plyasova, L. M.; Polukhina, I. A.; Boronin, A. I. Metal-support interactions in Pt/Al₂O₃ and Pd/Al₂O₃ catalysts for CO oxidation. *Applied Catalysis B: Environmental* **2010**, *97*, 57-71.
- (117) Kibis, L. S.; Stadnichenko, A. I.; Koscheev, S. V.; Zaikovskii, V. I.; Boronin, A. I. Highly oxidized palladium nanoparticles comprising Pd⁴⁺ species: spectroscopic and structural aspects, thermal stability, and reactivity. *The Journal of Physical Chemistry C* **2012**, *116*, 19342-19348.
- (118) Baidya, T.; Bera, P.; Mukri, B.; Parida, S.; Kröcher, O.; Elsener, M.; Hegde, M. S. DRIFTS studies on CO and NO adsorption and NO plus CO reaction over Pd²⁺-substituted CeO₂ and Ce_{0.75}Sn_{0.25}O₂ catalysts. *Journal of Catalysis* **2013**, *303*, 117-129.
- (119) Chakarova, K.; Ivanova, E.; Hadjiivanov, K.; Klissurski, D.; Knözinger, H. Co-ordination chemistry of palladium cations in Pd-H-ZSM-5 as revealed by FTIR spectra of adsorbed and co-adsorbed probe molecules (CO and NO). *Physical Chemistry Chemical Physics* **2004**, *006*, 3702-3709.
- (120) Andonova, S.; Vovk, E.; Sjöblom, J.; Ozensoy, E.; Olsson, L. Chemical deactivation by phosphorous under lean hydrothermal conditions over Cu/BEA NH₃-SCR catalysts. *Applied Catalysis B: Environmental* **2014**, *147*, 251-263.
- (121) Hegedus, L. L.; Baron, K. Phosphorus accumulation in automotive catalysts. *Journal of Catalysis* **1978**, *54*, 115-119.
- (122) Xie, L.; Liu, F.; Shi, X.; Xiao, F.-S.; He, H. Effects of post-treatment method and Na cation on the hydrothermal stability of Cu-SSZ-13 catalyst for the selective catalytic reduction of NO_x with NH₃. *Applied Catalysis B: Environmental* **2015**, *179*, 206-212.
- (123) Zhao, Z.; Yu, R.; Zhao, R.; Shi, C.; Gies, H.; Xiao, F.-S.; De Vos, D.; Yokoi, T.; Bao, X.; Kolb, U.; Feyen, M.; McGuire, R.; Maurer, S.; Moini, A.; Müller, U.; Zhang, W. Cu-exchanged Al-rich SSZ-13 zeolite from organotemplate-free synthesis as NH₃-SCR catalyst: Effects of Na⁺ ions on the activity and hydrothermal stability. *Applied Catalysis B: Environmental* **2017**, *217*, 421-428.
- (124) van der Bij, H. E.; Weckhuysen, B. M. Phosphorus promotion and poisoning in zeolite-based materials: synthesis, characterisation and catalysis. *Chemical Society Reviews* **2015**, *44*, 7406-7428.
- (125) Briggs, D. Handbook of X-ray Photoelectron Spectroscopy C. D. Wanger, W. M. Riggs, L. E. Davis, J. F. Moulder and G. E. Muilenberg Perkin-Elmer Corp., Physical Electronics

Division, Eden Prairie, Minnesota, USA, 1979. 190 pp. \$195. *Surface and Interface Analysis* **1981**, 3, v-v.

(126) Shwan, S.; Jansson, J.; Olsson, L.; Skoglundh, M. Chemical deactivation of Fe-BEA as NH₃-SCR catalyst—Effect of phosphorous. *Applied Catalysis B: Environmental* **2014**, 147, 111-123.

(127) Kröger, V.; Hietikko, M.; Angove, D.; French, D.; Lassi, U.; Suopanki, A.; Laitinen, R.; Keiski, R. L. Effect of phosphorus poisoning on catalytic activity of diesel exhaust gas catalyst components containing oxide and Pt. *Topics in Catalysis* **2007**, 42, 409-413.

(128) Jeong, J. M.; Park, J. H.; Baek, J. H.; Hwang, R. H.; Jeon, S. G.; Yi, K. B. Effect of acid treatment of Fe-BEA zeolite on catalytic N₂O conversion. *Korean Journal of Chemical Engineering* **2017**, 34, 81-86.

(129) Bernhard, M.; Reschetilowski, W.; Paasch, S. Spectroscopic study of phosphorus modified H-ZSM-5. *Microporous and Mesoporous Materials - MICROPOROUS MESOPOROUS MAT* **2011**, 142, 178-183.

(130) Müller, D.; Grunze, I.; Hallas, E.; Ladwig, G. Hochfeld-²⁷Al-NMR-Untersuchungen zur Aluminiumkoordination in Kristallinen Aluminiumphosphaten. *Zeitschrift für anorganische und allgemeine Chemie* **1983**, 500, 80-88.